The acid-base-nucleophile catalytic triad in ABH-fold enzymes is coordinated by a set of structural elements

Alexander Denesyuk[1,2]☯*, **Polytimi S. Dimitriou**[1]☯, **Mark S. Johnson**[1],
Toru Nakayama[3], **Konstantin Denessiouk**[1]

1 Structural Bioinformatics Laboratory, Biochemistry, Faculty of Science and Engineering, Åbo Akademi University, Turku, Finland, **2** Institute for Biological Instrumentation of the Russian Academy of Sciences, Federal Research Center "Pushchino Scientific Center for Biological Research of the Russian Academy of Sciences", Pushchino, Russia, **3** Department of Biomolecular Engineering, Graduate School of Engineering, Tohoku University, Sendai, Miyagi, Japan

☯ These authors contributed equally to this work.
* adenesyu@abo.fi

Abstract

The alpha/beta-Hydrolases (ABH) are a structural class of proteins that are found widespread in nature and includes enzymes that can catalyze various reactions in different substrates. The catalytic versatility of the ABH fold enzymes, which has been a valuable property in protein engineering applications, is based on a similar acid-base-nucleophile catalytic mechanism. In our research, we are concerned with the structure that surrounds the key units of the catalytic machinery, and we have previously found conserved structural organizations that coordinate the catalytic acid, the catalytic nucleophile and the residues of the oxyanion hole. Here, we explore the architecture that surrounds the catalytic histidine at the active sites of enzymes from 40 ABH fold families, where we have identified six conserved interactions that coordinate the catalytic histidine next to the catalytic acid and the catalytic nucleophile. Specifically, the catalytic nucleophile is coordinated next to the catalytic histidine by two weak hydrogen bonds, while the catalytic acid is directly involved in the coordination of the catalytic histidine through by two weak hydrogen bonds. The imidazole ring of the catalytic histidine is coordinated by a CH-π contact and a hydrophobic interaction. Moreover, the catalytic triad residues are connected with a residue that is located at the core of the active site of ABH fold, which is suggested to be the fourth member of a "structural catalytic tetrad". Besides their role in the stability of the catalytic mechanism, the conserved elements of the catalytic site are actively involved in ligand binding and affect other properties of the catalytic activity, such as substrate specificity, enantioselectivity, pH optimum and thermostability of ABH fold enzymes. These properties are regularly targeted in protein engineering applications, and thus, the identified conserved structural elements can serve as potential modification sites in order to develop ABH fold enzymes with altered activities.

Introduction

The structural family of alpha/beta-Hydrolases (ABH) includes enzymes that are widely found in nature and have diverse functions, such as esterases, lipases, thioesterases, amidases, epoxide hydrolases, dehalogenases, haloperoxidases, and hydroxynytrile lyases [1–3]. Because of their remarkable catalytic versatility, the ABH fold enzymes have often served as targets in protein engineering applications for the development of biocatalysts with improved characteristics [4]. Nevertheless, the ability of the ABH fold enzymes to catalyze various reactions in different substrates is based on a similar acid-base-nucleophile catalytic mechanism that is located at the core of the ABH fold [5–7].

The ABH fold is shaped by a β-sheet of eight mostly parallel β-strands, with the exception of the antiparallel strand β2, and is surrounded by six α-helices that are arranged in an α-turn-β supersecondary structure geometry, starting with αA helix that is situated before strand β4. Helical caps and other domains can be inserted in the fold, yet it is the ABH fold structure that comprises the catalytic domain of the ABH enzymes, with the residues of the acid-base-nucleophile catalytic mechanism being located at conserved positions across the ABH fold (Fig 1) [1, 6, 7]. Particularly, the catalytic acid is usually located at the turn after strand β7 (in the group A of the ABH fold enzymes) or alternatively, at the C-terminus of strand β6 (in the group B); the catalytic base, a conserved histidine, is located at a flexible loop after strand β8; and the catalytic nucleophile is located at the apex of a sharp turn at the C-terminus of strand β5, at a conserved structure called "nucleophile elbow" that retains structural and sequence conservation (G-X-Nuc-X-G motif). Located opposite to the catalytic triad, the oxyanion hole is usually shaped by two residues, one of which follows the catalytic nucleophile and the second is located at the C-terminus of strand β3 [1, 6, 7].

Based on the findings of our previous research, it appears that the invariable arrangement of the residues of the catalytic triad and the oxyanion hole on the ABH fold is not the only conserved structural feature of the catalytic mechanism of ABH fold enzymes. Indeed, in our research, where we are concerned with the structural conservation of the catalytic core of ABH fold enzymes, we have previously found that the residues involved in the catalytic machinery, which are located within the same plane of the β-sheet, not only maintain their structural positions on the ABH fold but are also surrounded by conserved, planar geometries [8, 9]. Specifically, "the catalytic acid zone" [8], "the nucleophile zone" [9] and "the oxyanion zone" [9] coordinate the catalytic acid, the catalytic nucleophile and the residues of the oxyanion hole respectively in the optimal arrangement that is required to achieve enzymatic activity. The planar zones are located at the C-termini of the strands of the β-sheet: the catalytic acid zone is formed by residues at the C-terminus of strand β7 and β6, while the nucleophile zone is formed by residues at the C-termini of strands β5 and β3 and overlaps with the oxyanion zone, which is formed by residues at the C-termini of strands β3 and β4.

In addition to the coordination of the catalytic acid, the catalytic nucleophile and the residues of the oxyanion hole, we have found that the catalytic acid zone, the nucleophile zone and the oxyanion zone indirectly affect the coordination of the catalytic histidine [8, 9]. In particular, we have shown that the catalytic acid zone is connected to the loop fragment prior to the catalytic histidine, and that conserved aromatic residues from the nucleophile zone and the oxyanion zone can interact with residues at the loop fragment that follows the catalytic histidine. We have deduced that the three planar zones have a cooperative effect on the stabilization of the flexible loop that hosts the catalytic histidine, regulating its position on top of the β-sheet and close to the catalytic acid and the catalytic nucleophile. The interactions that involve the loop fragments that precede and follow the catalytic histidine are complementary to the well-known, conserved weak-hydrogen bond that is observed in serine hydrolases [10], which

Alpha/beta-Hydrolases fold enzymes

Strand 8

Strand 7

Acid zone

Acid (group A)

X(acid+2)

Base

Acid (group B)   IV

X(IV+1)

X(acid+3)

Strand 6

X(IV+2)

Nucleophile

XoxyI

Strand 5

X(nuc+4)

XoxyII

Nucleophile zone

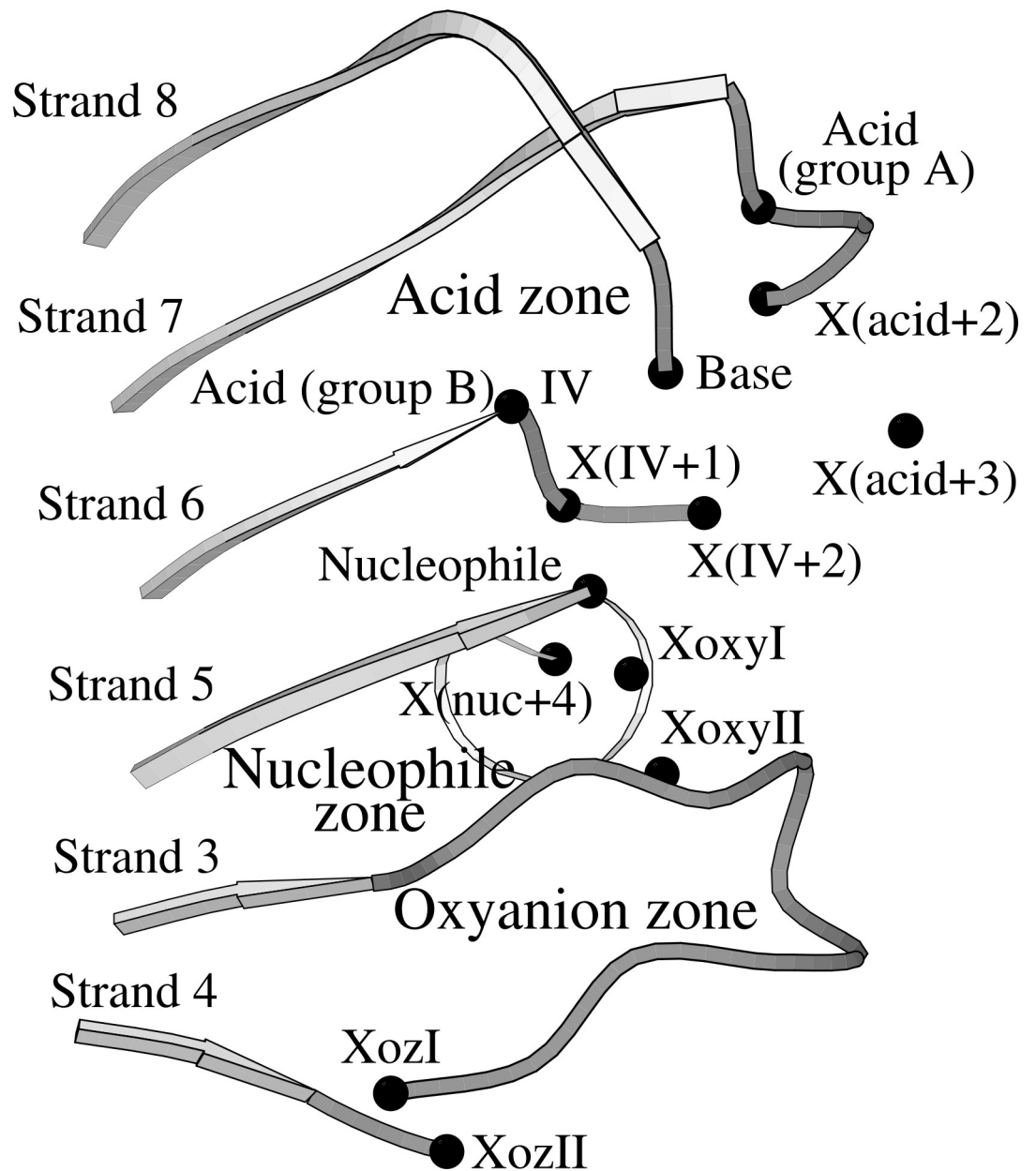Strand 3

Oxyanion zone

Strand 4

XozI

XozII

Fig 1. Conserved structural motifs at the catalytic site of ABH fold enzymes. Most key features of the catalytic machinery are coordinated by conserved structural organizations within the same plane as the central β-sheet of the ABH fold. Specifically, the catalytic acid ("Acid"), which is located at the turn that follows strand β7 ("group A") or at the C-terminus of strand β6 ("group B", position "IV"), is coordinated by the structural organization that is called "Catalytic acid zone" ("Acid zone"), while the catalytic nucleophile ("Nucleophile") and the two residues that help form the oxyanion hole ("XoxyI" and "XoxyII") are coordinated by the overlapping "Nucleophile zone" and "Oxyanion zone". The catalytic histidine ("Base") is located at a flexible loop that follows strand β8 and is linked with the β-sheet at the C-terminus of strand β6. The residues of the catalytic machinery, two conserved residues of Oxyanion zone ("XozI" and "XozII"), four residues of catalytic acid loops ("X(acid+2)", "X(acid+3)", "X(IV+1)" and "X (IV+2)") and one residue of the nucleophile elbow ("X(nuc+4)") are indicated with black dots.

anchors the imidazole ring of the catalytic histidine at the β-sheet by interacting with the main-chain oxygen of the residue at the C-terminus of strand β6.

So far, our comparative analysis of the structural core of ABH fold enzymes has been successful in identifying conserved, structural organizations that coordinate the units of the catalytic mechanism that are situated at the β-sheet. But, unlike the other residues of the catalytic mechanism, the catalytic histidine cannot be coordinated by a closed, structural organization because it is located at a flexible loop, and thus, a reasonable question is to ask whether there are structural elements that coordinate the catalytic histidine next to the other residues of the catalytic triad in addition to the direct and indirect interactions that we have mentioned above.

To address this question, we have focused here on the local structure around catalytic histidine, seeking for structural determinants that govern the fine tuning of the catalytic residues with respect to each other. The comparative analysis of the active sites of representative ABH structures has revealed several conserved structural elements that coordinate and properly orient the catalytic histidine next to the catalytic acid and the catalytic nucleophile. Even more so, it seems that several of the conserved structural elements that coordinate the residues of the catalytic mechanism, are routinely involved in ligand binding. Altogether, the results of this comprehensive study complete our structural description of the catalytic structural core of the ABH fold. Combined with information that arise from sequence comparisons and experimental data, we expect that the complete, structural mapping of the active site framework of ABH fold enzymes will help to shed light on the factors that affect the enzymatic activity, and potentially advance the utility of ABH fold enzymes in protein engineering applications.

Results

As we have reviewed in the Introduction section, the residues of the acid-base-nucleophile catalytic triad of the ABH fold enzymes are located at conserved positions across the ABH fold: the catalytic acid and the catalytic nucleophile are located at the same plane with the β-sheet, while the catalytic base, a conserved histidine, is located outside this plane, but directly interacts with the other two catalytic residues. In our previous research, we have identified the conserved structural elements that coordinate the planar catalytic residues. Here, we have searched for conserved structural elements that coordinate the catalytic histidine, located next to both the catalytic acid and the catalytic nucleophile by comparing representative structures from the 40 ABH fold enzyme families of the Structural Classification of Proteins (SCOP) database [11], obtained from the Protein Data Bank (PDB) [12].

In order to explore the coordination of the catalytic histidine relative to the catalytic nucleophile and the catalytic acid, our comparative analysis has been conducted in two parts: the first part is concerned with the structure around the catalytic nucleophile-base pair, and the second part is concerned with the structure that surrounds the catalytic acid-base pair. The findings of this analysis are also presented in two parts: in the first part, we introduce the conserved structural elements that are involved in the coordination of the catalytic nucleophile next to the catalytic histidine, while in the second part, we revisit the area that surrounds the catalytic acid zone and the conserved structural elements that coordinate the catalytic acid next to the catalytic histidine. Additional conserved structural elements that are located at the active site of ABH enzymes, but are not involved in the coordination of the catalytic residues, are mentioned in both parts.

Lastly, we introduce our findings from the comparison of the active sites of ligand-bound ABH structures, where we have found that several of the conserved structural elements that

are involved in the coordination of the catalytic residues also participate in the binding of the ligand.

Coordination of the catalytic nucleophile next to the catalytic histidine

Our search for structural elements that support the contact between the catalytic nucleophile and the catalytic histidine is focused on the area where the two catalytic residues normally interact, i.e. around the C-termini of strands β5 and β6 (Fig 1). The C-terminus of strand β5 is part of the characteristic ABH-fold structural motif, known as "the nucleophile elbow", with the catalytic nucleophile being located at the apex of the sharp turn that occurs at the C-terminus of strand β5. The C-terminus of strand β6 is situated parallel to the nucleophile elbow, followed by a similar sharp turn; the residue that is located at the apex of the sharp turn forms a weak hydrogen bond with the catalytic histidine, linking the imidazole ring with the β-sheet, as is often seen in serine hydrolases [10]; this same residue is a structural element of the catalytic acid zone, located at the position called "position IV" [8]. In most ABH fold families, the residue at position IV is in contact with the catalytic acid that is located at the turn after strand β7, but it is possible for the catalytic acid to alternately occur at position IV.

The comparison of the geometries near the edges of strands β5 and β6 in representative structures from 40 ABH fold enzyme families has revealed two conserved, weak hydrogen bonds that coordinate the catalytic nucleophile next to the catalytic histidine, through the connection of the catalytic nucleophile with positions IV and IV+1 located at the C-terminus of strand β6, which we refer to as "residue X_{IV}" and "residue X_{IV+1}" (Table 1).

In the carboxylesterase SshEstI [13] (Fig 2), for example, the catalytic nucleophile Ser151 forms two weak hydrogen bonds with its neighboring residues: one bond with $Tyr177_{IV}$ (CA/Ser151 –O/Tyr177) and a second bond with $Pro178_{IV+1}$ (O/Ser151 –CA/Pro178). The former contact, the weak hydrogen bond between the catalytic nucleophile (Ser151) and the residue at position IV (Tyr177), coordinates the catalytic nucleophile next to the catalytic histidine, because the main-chain oxygen atom of $Tyr177_{IV}$ also forms the already-reported [10], conserved interaction with the catalytic histidine (O/Tyr177 –CE1/His274). The second weak hydrogen bond observed between the catalytic nucleophile and residue X_{IV+1} is involved in the coordination of the catalytic nucleophile.

The two weak hydrogen bonds between the catalytic nucleophile with residue X_{IV} and residue X_{IV+1} are absolutely conserved in all 40 ABH fold enzyme families (Table 1). Because both interactions involve main-chain atoms, the identified hydrogen-bonding scheme is not affected when the catalytic acid occurs at the C-terminus of strand β6, while it also remains intact regardless of the type of amino acids that occur at positions IV and IV+1. Specifically, residue X_{IV} is often occupied by a small amino acid (glycine in 7 of 40 ABH fold enzyme families) or a hydrophobic amino acid (16 ABH fold families), however bulky side chains such as tyrosine (2 ABH fold families) or arginine (2 ABH fold families) are tolerated at position IV, too. Residue X_{IV+1} is much more conserved than residue X_{IV}, and is most commonly a glycine (16 of 40 ABH fold families) or a proline (12 ABH fold families).

Besides the two weak hydrogen bonds that coordinate the catalytic nucleophile-histidine pair, in our search for structural elements at the C-termini of strand β5 and strand β6, we have identified an additional conserved weak hydrogen bond that occurs in the vast majority of ABH enzyme families (Table 1). While not involved in the coordination of the catalytic residues, the contact CB/N155 –O/A179 in SshEstI (Fig 2) links two residues that are situated at the core of the active site: the residue that is located 4 positions after the catalytic nucleophile ($Asn155_{nuc+4}$ in SshEstI) with the residue that is located at position IV+2 ($Ala179_{IV+2}$ in

Table 1. Inventory of interactions that participate in the proper positioning of the catalytic histidine next to the catalytic nucleophile in 40 ABH fold enzyme families. The main-chain oxygen atom of residue X_{IV} interacts with both the catalytic histidine and the catalytic nucleophile (column CA/Nucleophile–O/X_{IV}), orienting the imidazole ring of the catalytic histidine with respect to the side-chain of the catalytic nucleophile. Residue X_{IV+1} also interacts with the catalytic nucleophile (column O/Nucleophile–CA/X_{IV+1}) and thus, has an indirect influence on the optimal arrangement of the catalytic histidine-nucleophile pair. Unrelated to the coordination of the catalytic residues, an additional conserved contact (column Sc/(Nucleophile+4)–O/X_{IV+2}) is formed between the residue that is located four positions after the catalytic nucleophile and the residue that is located two positions after residue X_{IV}; this conserved contact is formed close to the catalytic nucleophile, residue X_{IV} and residue X_{IV+1}. In the second row of the table, the interactions from the carboxylesterase SshEstI (SCOP family #2, PDB ID:3WJ1_A) are listed, corresponding to the interactions that are illustrated in Fig 2. In four ABH fold families [SCOP families #12 (PDB ID:1MJ5_A), #23, #27 and #29], residue X_{IV} is the catalytic acid residue. SCOP family #12 is represented by two structures in order to properly reflect the local structural variations in ABH fold enzymes that have their catalytic acid at the canonical position (i.e. at the turn that follows strand β7, e.g. structure PDB ID:1B6G_A) or at the alternate position (i.e. at the position of residue X_{IV}, e.g. structure PDB ID:1MJ5_A). Alternative types of contacts to those described as conserved occur in a few representative structures, for example in ABH fold enzyme families of Epoxide hydrolase (SCOP family #18), Atu1826-like (SCOP family #36) and PHB depolymerase-like (SCOP family #37). Values in parentheses correspond to the distances of the hydrogen bond to the hydrogen atom.

SCOP family # / SCOP family name	PDB ID Reference	CA/Nucleophile–O/X_{IV}	O/Nucleophile–CA/X_{IV+1}	Sc/(Nucleophile+4)–O/X_{IV+2}
2. Carboxylesterase	3WJ1_A [13]	CA/S151-O/Y177 3.2 (2.2)	O/S151-CA/P178 3.6 (2.6)	CB/N155-O/A179 3.0 (2.2) ND2/N155-O/A179 3.0
1. Acetylcholinesterase-like	1QE3_A [82]	CA/S189-O/S215 3.2 (2.2)	O/S189-CA/G216 3.8 (2.8)	CA/M193-O/A217 3.2 (2.2) CG/M193-O/A217 3.4 (2.6)
2. Carboxylesterase	1LZL_A [83]	CA/S160-O/I188 3.0 (2.0)	O/S160-CA/P189 3.6 (2.6)	CA/G164-O/E190 3.1 (2.3)
3. Mycobacterial antigens	1DQZ_A [84]	CA/S124-O/S148 3.3 (2.3)	O/S124-CA/G149 3.5 (2.4)	CA/G128-O/F150 4.6 (3.7)
4. Hypothetical protein TT1662	1UFO_A [85]	CA/S113-O/I136 3.4 (2.4)	O/S113-CA/G137 4.4 (3.5)	CA/F117-O/S138 3.5 (2.7) CD1/F117-O/S138 3.4 (2.4)
5. PepX catalytic domain-like	3PUI_A [86]	CA/S117-O/M141 3.2 (2.2)	O/S117-CA/A142 4.5 (3.7)	CA/V121-O/S143 4.0 (3.1) CG1/V121-O/S143 3.8 (2.9) CG2/V121-O/S143 3.6 (2.6)
6. Prolyl oligopeptidase, C-terminal domain	1H2W_A [87]	CA/S554-O/V578 3.1 (2.1)	O/S554-CA/G579 3.4 (2.4)	CB/L558-O/V580 3.4 (2.5) CD1/L558-O/V580 3.6 (2.7)
7. DPP6 catalytic domain-like	1ORV_A [88]	CA/S630-O/A654 3.3 (2.3)	O/S630-CA/P655 3.6 (2.5)	CB/Y634-O/V656 3.4 (2.7) CD1/Y634-O/V656 3.1 (2.1)
8. Serine carboxypeptidase-like	3SC2_A [89]	CA/S146-O/N176 3.1 (2.2)	O/S146-CA/G177 3.2 (2.6)	CA/G149-O/L178 3.3 (2.4)
9. Gastric lipase	1HLG_A [90]	CA/S153-O/A180 3.4 (2.5)	O/S153-CA/P181 4.9 (4.1)	CB/T157-O/V182 2.9 (1.9)
10. Proline aminopeptidase-like	1MTZ_A [91]	CA/S105-O/G129 3.0 (2.1)	O/S105-CA/G130 3.7 (2.7)	CB/A109-O/L131 3.3 (2.6)
11. Acetyl xylan esterase-like	1L7A_A [92]	CA/S181-O/Y204 3.2 (2.3)	O/S181-CA/P205 3.6 (2.7)	CA/G185-O/Y206 3.4 (2.7)
12. Haloalkane dehalogenase	1B6G_A [93]	N/D124-O/N148 2.8	O/D124-CB/A149 4.1 (3.5)	CA/F128-O/C150 3.6 (2.6) CD1/F128-O/C150 3.3 (2.3)
	1MJ5_A [94]	N/D108-O/E132 3.0	O/D108-CA/A133 4.6 (3.8)	CA/A112-O/I134 4.7 (4.0)
13. Dienelactone hydrolase	1ZI9_A [95]	CA/S123-O/Y145 3.3 (2.2)	O/S123-CA/G146 3.4 (2.3)	CB/A127-O/V147 3.5 (2.7)
14. Carbon-carbon bond hydrolase	2OG1_A [96]	CA/S112-O/G136 3.2 (2.4)	O/S112-CA/P137 3.7 (2.8)	CB/A116-O/G138 3.6 (2.6)
15. Biotin biosynthesis protein BioH	4ETW_A [39]	CA/A82-O/A106 3.4 (2.6)	O/A82-OG/S107 2.6	CD2/L86-O/S108 3.6 (2.8)
16. Aclacinomycin methylesterase RdmC	1Q0R_A [97]	CA/S102-O/L126 3.2 (2.1)	O/S102-CA/G127 4.0 (3.3)	OG1/T106-O/G128 4.4

(Continued)

Table 1. (Continued)

| SCOP family # / SCOP family name	PDB ID Reference	CA/Nucleophile–O/ X_{IV}	O/Nucleophile–CA/X_{IV} +1	Sc/(Nucleophile+4)–O/X_{IV} +2
17. Carboxylesterase/lipase	4DIU_A [98]	CA/S93-O/C115 3.2 (2.2)	O/S93-CA/A116 3.5 (2.6)	CG2/V97-O/P117 3.7 (3.1)
18. Epoxide hydrolase	1QO7_A [99]	CA/D192-CD2/L215 3.5	O/D192-CD2/L215 3.9 (2.9)	CB/S195-O/L215 3.5 (2.8)
19. Haloperoxidase	1BRT_A [100]	CA/S98-O/A123 3.1 (2.2)	O/S98-CA/S124 4.3 (3.2)	OG1/T101-N/L125 3.2
20. Thioesterases	1EI9_A [101]	CA/S115-O/G140 3.6 (2.5)	O/S115-CA/G141 3.4 (2.4)	OE1/Q119-N/Q142 2.8 ND2/Q119-O/Q142 3.8
21. Carboxylesterase/ thioesterase 1	1FJ2_A [102]	CA/S114-O/S138 3.2 (2.3)	O/S114-CB/C139 3.1 (2.6)	CA/A118-O/W140 3.1 (2.3)
22. Ccg1/TafII250-interacting factor B (Cib)	1IMJ_A [103]	CA/S111-O/A135 3.3 (2.3)	O/S111-CA/P136 3.4 (2.5)	CA/G114-O/I137 3.6 (2.7)
23. A novel bacterial esterase	1QLW_A [104]	CA/S206-O/E230 3.2 (2.3)	O/S206-CA/P231 3.7 (2.8)	O/S206-N/G232 2.9
24. Lipase	1JFR_A [105]	CA/S131-O/T154 3.2 (2.2)	O/S131-CA/G155 3.5 (2.5)	CA/G135-O/W156 3.3 (2.3)
25. Fungal lipases	1TCA_A [106]	CA/S105-O/A132 3.3 (2.4)	O/S105-CA/P133 3.7 (2.6)	CD2/L109-O/D134 4.0 (3.0) CB/L109-OD1/D134 3.8 (3.0)
26. Bacterial lipase	1ISP_A [107]	CA/S77-O/G103 3.3 (2.3)	O/S77-CA/G104 3.4 (2.4)	CB/A81-O/A105 3.3 (2.2)
27. Pancreatic lipase, N-terminal domain	1BU8_A [108]	CA/S152-O/D176 3.4 (2.6)	O/S152-CA/P177 3.7 (2.7)	NE2/H156-O/A178 2.7
28. Hydroxynitrile lyase-like	3C6X_A [109]	CA/S80-O/N104 3.1 (2.4)	O/S80-CA/S105 3.2 (2.5)	CA/G83-O/V106 3.4 (2.5)
29. Thioesterase domain of polypeptide, polyketide and fatty acid synthases	1JMK_C [110]	CA/S80-O/D107 5.5 (4.7)	O/S80-OG/S108 3.1	CB/S84-O/Y109 5.1 (4.1)
30. Cutinase-like	1BS9_A [111]	CA/S90-O/G132 3.4 (2.3)	O/S90-CA/D133 4.0 (2.9)	OE1/E94-CG/P134 3.5 (2.8)
31. YdeN-like	1UXO_A [112]	CA/S71-O/S97 3.6 (2.6)	O/S71-CA/G98 4.7 (3.7)	CB/P75-O/F99 3.6 (2.8) CD/P75-O/F99 3.5 (2.6)
32. Putative serine hydrolase Ydr428c	1VKH_A [113]	CA/S110-O/D151 3.3 (2.4)	O/S110-CA/G152 3.7 (2.7)	OG1/T114-O/I153 2.7 CG2/T114-O/I153 3.3 (2.5)
33. Acylaminoacid-releasing enzyme, C-terminal domain	1VE6_A [114]	CA/S445-O/A469 3.1 (2.2)	O/S445-CA/S470 3.9 (2.8)	CA/Y449-O/V471 3.7 (2.8) CD1/Y449-O/V471 3.3 (2.2)
34. Hypothetical esterase YJL068C	1PV1_A [115]	CA/S161-O/A187 3.1 (2.1)	O/S161-CA/P188 3.6 (2.6)	CB/Y165-O/I189 3.0 (1.9) CD1/Y165-O/I189 3.5 (2.9)
35. Hypothetical protein VC1974	1R3D_A [116]	CA/S91-O/G118 3.4 (2.4)	O/S91-CA/G119 3.7 (2.9)	CG/R95-O/H120 3.4 (2.6) CD/R95-O/H120 3.3 (2.8)
36. Atu1826-like	2I3D_A [117]	CA/S108-O/A131 3.3 (2.2)	O/S108-CA/P132 4.5 (3.4)	W112-Y137 stacking
37. PHB depolymerase-like	2D80_A [118]	CA/S39-O/A64 3.3 (2.5)	O/S39-CA/G65 3.9 (3.2)	Y43-G66 stacking
38. IroE-like	2GZR_A [14]	CA/S189-O/S212 3.2 (2.2)	O/S189-CA/P213 3.4 (2.4)	CD1/L193-O/S214 3.7 (2.6) CD2/L193-O/S214 3.9 (3.0)
40. O-acetyltransferase	2B61_A [119]	CA/S143-O/C167 3.5 (2.6)	O/S143-CB/S168 3.2 (2.4)	CG/M147-O/S169 3.8 (3.1) CE/M147-O/S169 3.5 (3.1)
41. 2,6-dihydropseudo-oxynicotine hydrolase-like	2JBW_A [120]	CA/S217-O/G240 3.2 (2.2)	O/S217-CA/G241 3.2 (2.2)	CB/N221-O/F242 3.2 (2.5) ND2/N221-O/F242 2.9
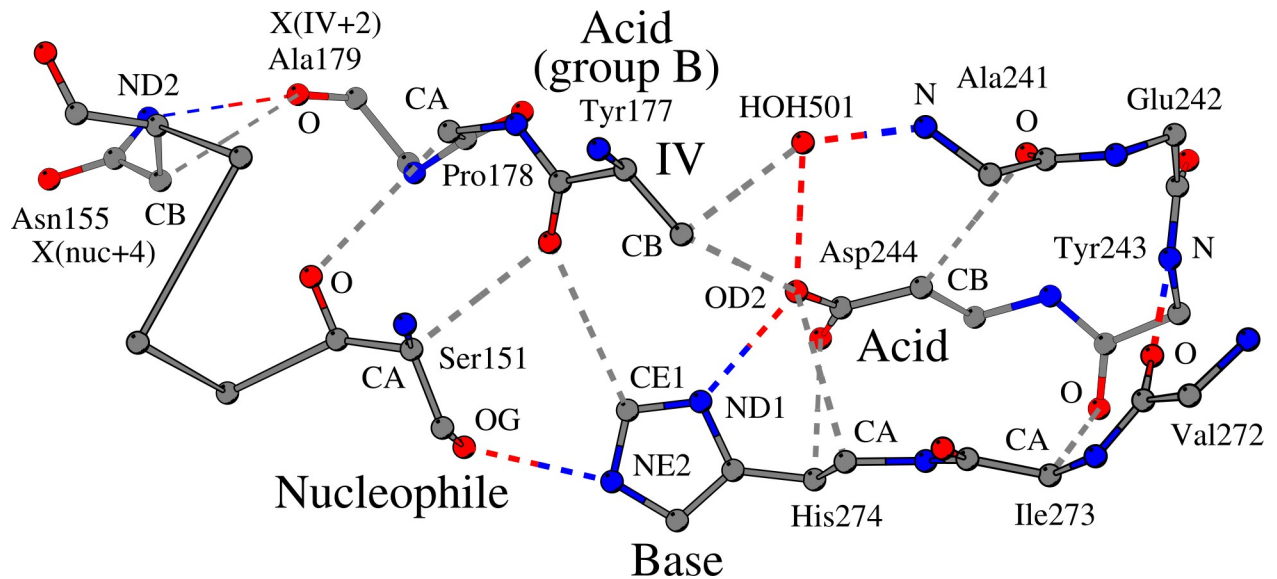
Fig 2. Coordination of the catalytic nucleophile-histidine pair and the catalytic histidine-acid pair in the carboxylesterase SshEstI (PDB ID:3WJ1). The catalytic nucleophile ("Nucleophile", Ser151 in SshEstI) is hydrogen bonded (OG/Ser151 –NE2/His274) to the catalytic histidine ("Base", His274 in SshEstI) as part of the standard interaction network of the residues of the catalytic machinery. However, three additional conserved interactions ensure the fine turning of the two catalytic residues next to each other: The main-chain oxygen atom of Tyr177 that is located at the C-terminus of strand β6 (termed and shown as "IV") forms two weak hydrogen bonds: one with the catalytic nucleophile (O/Tyr177 –CA/Ser151) and another with the catalytic histidine (O/Tyr177 –CE1/His274); a third contact (O/Ser151 –CA/Pro178) is formed between the catalytic nucleophile and Pro178 (located ahead of position IV) and coordinates the catalytic nucleophile. Thus, these three interactions support the optimal arrangement of the catalytic nucleophile-histidine pair. The catalytic histidine (His274) interacts (ND1/His274 –OD2/Asp244) with the catalytic acid ("Acid", Asp244 in SshEstI) and is further supported by two weak hydrogen bonds: OD2/Asp244 –CA/His274 and OD1/Asp244 –CB/His274. Interactions of the catalytic acid zone that are associated with the coordination of the catalytic histidine and other contacts located nearby the catalytic site are shown. Gray dashed lines, weak hydrogen bonds; colored dashed lines, standard hydrogen bonds.

SshEstI). Both residues are hydrophobic or aromatic in approximately 30 ABH enzyme families (Table 1).

The two weak hydrogen bonds formed between the catalytic nucleophile and residue X_{IV} and residue X_{IV+1} clearly serve to coordinate the catalytic nucleophile next to the catalytic histidine. The optimal arrangement of the catalytic nucleophile-histidine pair is additionally supported by the interaction of the nucleophile zone and the oxyanion zone with the loop fragment following the catalytic histidine, which helps stabilizing the flexible histidine loop located "above" the β-sheet. Likewise, on the other side of the catalytic machinery, the catalytic acid zone interacts with the loop fragment that precedes the catalytic histidine, fixing it close to the catalytic acid. Subsequently, we have performed a similar search for structural elements that coordinate the catalytic histidine next to the catalytic acid in the vicinity of the catalytic acid zone and, below, we show that conserved elements that contribute to the optimal arrangement of the catalytic acid-histidine pair.

Coordination of the catalytic acid next to the catalytic histidine

The interaction of the catalytic acid with the catalytic histidine takes place around the catalytic acid zone, near the C-termini of strand β6 and strand β7 [8], with the turn that follows strand β7 accommodating the catalytic acid residue in the majority of ABH fold enzyme families. As mentioned earlier, the catalytic acid zone helps stabilize the catalytic histidine loop, because the residue that precedes the catalytic acid interacts with the residue that is located two positions prior to the catalytic histidine.

Here, we have revisited the catalytic acid zone in order to search for structural elements that coordinate the catalytic acid next to the catalytic histidine. The comparative analysis of the active sites of enzymes from 40 ABH fold families has revealed four conserved interactions that fix the catalytic acid and the catalytic histidine in an optimal arrangement. Specifically, we have found two weak hydrogen bonds that are formed between the catalytic acid and the catalytic histidine (S1A Table), and two additional interactions that involve the imidazole ring of the catalytic histidine (column I set, S1B Table).

In SshEstI [13] for example (Fig 2), the catalytic acid Asp244 is coordinated next to the catalytic histidine by two weak hydrogen bonds: the first interaction is formed between the side-chain oxygen atom of Asp244 and the CA atom of His274 (CA/His274 –OD2/Asp244), while the second interaction links the other side-chain oxygen atom of Asp244 with the CB atom of His274 (CB/His274 –OD1/Asp244). The imidazole ring of His274 forms two contacts with two other neighboring residues (Fig 3). The first contact is a hydrophobic interaction between the catalytic His274 and Leu246 (CD1/Leu246 –CE1/His274); Leu246 is located at the catalytic acid turn, two sequence positions after the catalytic acid. The second contact is a CH–π interaction between His274 and Leu198 (CD2/Leu198 –π/His274); residue Leu198 is located at a flexible loop opposite to the β-sheet and is part of the helix-turn-strand supersecondary structure that connects strand β6 with strand β7.

The two weak hydrogen bonds formed between the catalytic acid and the catalytic histidine are observed in almost all ABH fold enzyme families regardless of the position of the catalytic acid (S1A Table), with the single exception of the hydrolase IroE from *Escherichia coli* (PDB ID:2GZR), which is suggested to have an atypical catalytic nucleophile-base dyad [14]. The interactions that involve the imidazole ring of the catalytic histidine are also recurrent in the 40 ABH fold enzyme families (column I set, S1B Table). The hydrophobic interaction is conserved in 32 ABH fold families; in 22 ABH fold families the interaction involves the residue that is located three positions after the catalytic acid (here termed residue X_{acid+3}), while in 7 ABH fold families the residue is located two positions after the catalytic acid (which we hereafter refer to as residue X_{acid+2}), for example Leu246$_{acid+2}$ in SshEstI. The CH–π interaction is conserved in 37 ABH fold families, with residue X_{acid+2} involved in the CH–π interaction with the imidazole ring in 29 ABH fold families, while in the remaining cases, the catalytic histidine interacts with some other neighboring residue, such as Leu198 in SshEstI. In the 22 of 40 ABH fold enzyme families, the imidazole ring of the catalytic histidine is simultaneously coordinated by a hydrophobic interaction with residue X_{acid+3} and a CH–π interaction with residue X_{acid+2}, while in 6 ABH fold enzyme families the imidazole ring is coordinated in a similar way to that observed in the reference structure SshEstI, which we have described in the previous paragraph.

Besides their role in the coordination of the catalytic residues, residue X_{acid+2}, residue X_{IV} and residue X_{IV+1} are linked through a separate hydrogen-bonding network (Fig 3), with residue X_{acid+2} (Leu246 in SshEstI) forming one weak hydrogen bond with residue X_{IV} (Tyr177 in SshEstI) and another weak hydrogen bond with residue X_{IV+1} (Pro178 in SshEstI). This interaction pattern is conserved in 35 of 40 ABH enzyme families (column II set, S1B Table).

In total, six conserved interactions coordinate the catalytic histidine next to the catalytic nucleophile and the catalytic acid at the active site of ABH fold enzymes. The conserved, structural elements that comprise the catalytic acid zone, the nucleophile zone and the oxyanion zone, together with the newly identified structural elements that coordinate the catalytic histidine, make up the catalytic structural core of the ABH fold enzymes. After perceiving the catalytic core as a composition of conserved structural elements, we have furthered our analysis to explore the role of the conserved structural core in ligand-bound ABH structures. As we show below, it appears that several elements of the conserved structural core not only contribute to
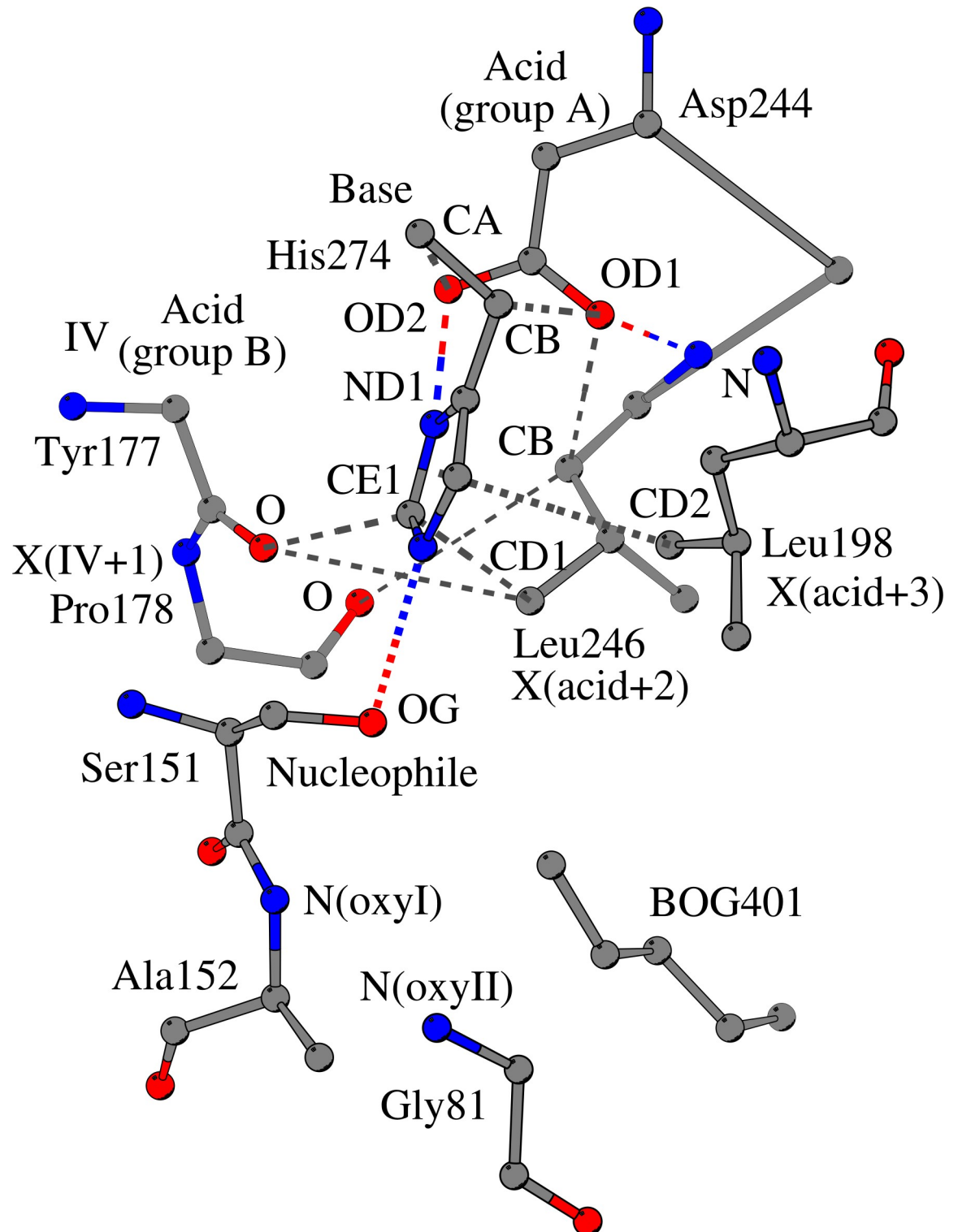
Fig 3. Coordination of the imidazole ring of the catalytic histidine in the carboxylesterase SshEstI (PDB ID:3WJ1). The optimal arrangement of catalytic residues requires the proper positioning of the imidazole ring of the catalytic histidine ("Base", His274 in SshEstI) relative to the side chains of the catalytic nucleophile ("Nucleophile", Ser151 in SshEstI) and the catalytic acid ("Acid", Asp244 in SshEstI). The catalytic histidine is anchored to the β-sheet through its contact with Tyr177 (position IV) and is directly coordinated by the catalytic acid Asp244. The imidazole ring of the catalytic histidine is coordinated by two interactions: a hydrophobic interaction (CD1/Leu246 –CE1/His274) with Leu246 (X(acid+2)), which is located two sequence positions after the catalytic acid, and a CH–π

interaction (CD2/Leu198 –π/His274) with Leu198 (X(acid+3)). The residues at the C-terminal end of strand β6, Tyr177 (IV) and Pro178 (IV+1), also interact with Leu246, which is situated at the turn that accommodates the catalytic acid. The residues, "OxyI" and "OxyII", which help form the oxyanion hole, and the bound ligand "BOG401" of carboxylesterase SshEstI are indicated. Gray dashed lines represent weak hydrogen bonds; colored dashed lines, standard hydrogen bonds.

the optimal arrangement of residues of the catalytic mechanism, but also engage in ligand binding.

Elements of the conserved, catalytic structural core of ABH fold enzymes participate in the binding of the ligand

Here, we define the catalytic structural core to be the geometry that is located at the active site of ABH fold enzymes and consists of the conserved structural elements that directly and indirectly coordinate the key units of the catalytic mechanism. In detail, the catalytic acid zone, the nucleophile zone, the oxyanion zone and the structural elements that are involved in the coordination of the catalytic histidine form a distinct interaction network that is common among the ABH fold enzyme families. The catalytic structural core extends through the whole area of the active site, which consequently raises the question of how the conserved geometry of the catalytic core correlates with the binding sites of ABH fold enzymes. Because ligand binding is highly dependent on both the structure of the ligand and the amino-acid variations of the protein interior, the comparison of the binding sites of the functionally diverse ABH fold enzymes appears to be counterintuitive. However, our attempt to compare the binding sites of ligand-bound ABH fold enzymes from 28 ABH fold enzyme families based on the conserved structural elements of the catalytic core has shown that the conserved structural elements of catalytic core often coincide with the residues that are involved in the binding of ligands, regardless of the structure of the ligand or the type of amino-acids that line the active sites of the ABH fold enzymes (Fig 4).

Starting with the catalytic acid zone, we have found that the catalytic acid does not participate in ligand binding (column Catalytic acid zone, Table 2). However, residue X_{acid+2} (Leu246 in SshEstI) and residue X_{acid+3}, which coordinate the imidazole ring of the catalytic histidine, routinely form contacts with the ligand in the majority of the ligand-bound ABH structures (column Catalytic acid zone, Table 2); the same applies for residues that are involved in the coordination of the imidazole ring but do not occur at conserved positions, such as Leu198 in SshEstI. Similarly, the catalytic histidine frequently interacts with the ligand (under Catalytic base loop in Table 2), sometimes accompanied by the residue that follows in sequence.

The search for ligand-binding interactions near the C-terminus of strand β6 has shown that residue X_{IV} (Tyr177 in SshEstI) and residue X_{IV+1} (Pro178 in SshEstI) occasionally participate in ligand binding, while residue X_{IV+2} (Ala179 in SshEstI) regularly interacts with the ligand (column Strand β6, Table 2).

In the vicinity of the nucleophile zone and the oxyanion zone, we have found several residues that are involved in ligand binding, with some of them belonging to the conserved catalytic core and others being located at a fixed distance from conserved structural elements of the catalytic core (column Oxyanion zone and column Nucleophile zone, Table 2). Within the nucleophile zone, residues of the nucleophile elbow that interact with the ligand in the majority of ligand-bound ABH structures (column Nucleophile zone, Table 2) include the catalytic nucleophile and the following residue (one of the two oxyanion hole-forming residues). The other residues of the nucleophile elbow rarely participate in ligand binding, except for the residue prior to the catalytic nucleophile. Because of its location at the active site, the residue that
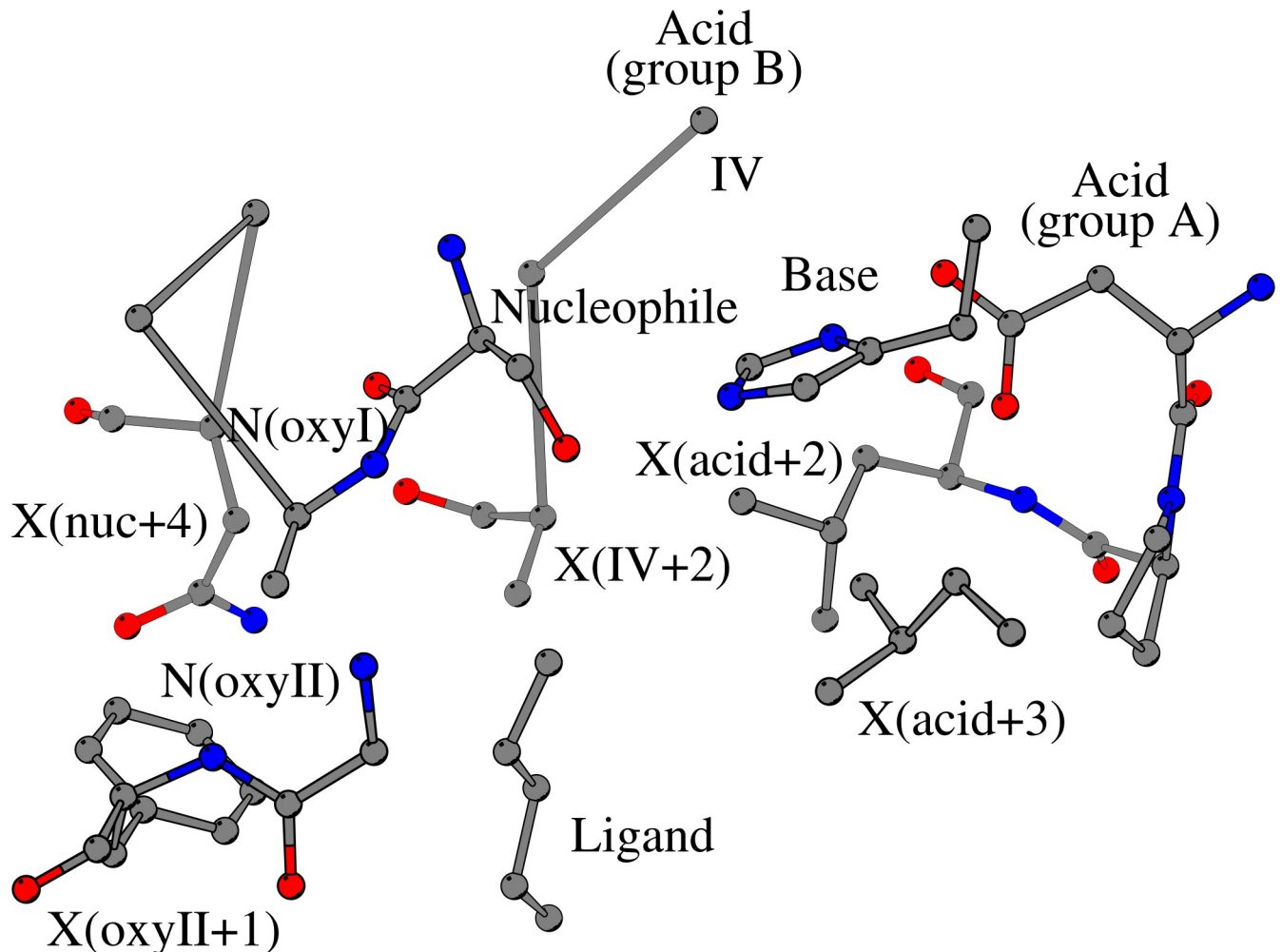
Fig 4. Structural elements at the active site of the ABH fold enzymes surround the bound ligand. Recognized substrate molecules (shown as "Ligand") are bound to the active sites of ABH fold enzymes in order to be hydrolyzed. Key residues of the catalytic machinery, such as the catalytic histidine ("Base"), the catalytic nucleophile ("Nucleophile") and the residues that help form the oxyanion hole ("oxyI" and "oxyII") often interact with the bound substrate; the catalytic acid, either at its canonical position (at the turn that follows strand β7, "Acid (group A)") or at its alternate position (at the C-terminal end of strand β6, "Acid (group B)") does not participate in ligand binding. Several residues, which belong to the structural core of ABH fold enzymes, participate both in the coordination of the residues of the catalytic machinery and in ligand binding, including the residues that are located two and three sequence positions after the catalytic acid, illustrated as "X(acid+2)" and "X(acid+3)" respectively, and the residue at the C-terminus of strand β6. Other residues, usually comprising the substrate binding core, are illustrated as "X(IV+2)" for the residue that is located two positions after the C-terminus of strand β6, "X(oxyII +1)" for the residue that follows the second residue that helps form the oxyanion hole, and "X(nuc+4)" for the residue that is located four positions after the catalytic nucleophile.

is situated four sequence positions after the catalytic nucleophile ($Asn155_{nuc+4}$ in SshEstI) can interact with the ligand, too. Within the oxyanion zone, the second residue of the oxyanion hole commonly binds the ligand (column Oxyanion zone, Table 2), with the preceding and following residues having a major involvement in ligand binding in general.

Most of the 28 sampled ABH fold enzyme families are represented by a single ligand-bound structure, however for three of the 28 ABH fold families, we have found more than one ligand-bound structure. Thus, we have obtained three ligand-bound structures for the ABH fold enzyme family of haloalkane dehalogenases (SCOP family #12), two ligand-bound structures for the ABH fold enzyme family of biotin biosynthesis protein BioH (SCOP family #15), and two ligand-bound structures for the ABH fold enzyme family of epoxide hydrolases (SCOP

Table 2. Elements of the conserved catalytic structural core are involved in ligand binding in 28 ABH fold enzyme families. In ligand-bound represenative structures, the recognized substrate molecule (Ligand) frequently interacts with residues that belong to the conserved structural organizations of the ABH fold, including the oxyanion zone (Oxyanion zone), the nucleophile zone (Nucleophile zone), the C-terminal end of strand β6 (Strand β6) and the catalytic acid zone (Catalytic acid zone); residues from the loop that accommodates the catalytic histidine (Catalytic base loop) can also participate in ligand binding. Two ABH fold enzyme families (SCOP family #15 and SCOP family #18) are represented by two structures, each bound to a different substrate, while one ABH fold enzyme family (SCOP family #12) is represented by three representative structures that are bound to three different substrates. The first entry is for carboxylesterase SshEstI (SCOP family #2, PDB ID:3WJ1_A). Residues that are in bold signify that the specific residue does not belong to the conserved catalytic core, but are adjacent to it. Fields of the table that contain the entry "None" indicate that the corresponding geometry does not participate in ligand binding.

SCOP family # / SCOP family name	PDB ID Reference	Ligand	Oxyanion zone	Nucleophile zone	Strand β6	Catalytic acid zone	Catalytic base loop
2. Carboxylesterase	3WJ1_A [13]	BOG 401_A	G81, F82	S151, A152	**A179**	L198, L246	None
2. Carboxylesterase	1LZK_A [83]	CAC 500_A	G87, G88, G89	Q159, S160, A161	**E190**	W209, L262	H290
3. Mycobacterial antigens	1DQY_A [84]	DEP 401_A	G39, L40, R41	L123, S124, M125	**F150**	L227	None
5. PepX catalytic domain-like	3I2K_A [121]	DBC 591_A	Y44	S117, Y118, **V121**	None	F261, L407	H287
6. Prolyl oligopeptidase, C-terminal domain	2XDW_A [122]	PHQ 791_P PRO 792_P YCP 793_P	Y473, F476, I478	S554, N555	**V580**	R643, V644	H680
7. DPP6 catalytic domain-like	2AJ8_A [123]	SC3 1601_A	V546, Y547	W629, S630, Y631	**V656**	N710, V711	H740
8. Serine carboxypeptidase-like	1WHT_A, B [124]	BZS 430_A	N51, G52, G53, C56	E145, S146, Y147	None	Y239, V340	H397, E398
10. Proline aminopeptidase-like	1MT3_A [91]	MES 200_A	G36, G37	S105, Y106	**L131**	E245, V246	H271, L272
11. Acetyl xylan esterase-like	1ODT_C [125]	ACT 1318_C	G90, Y91, A93	A181, Q182	**Y206**	V271	H298
12. Haloalkane dehalogenase	1BE0_A [126]	ACY 401_A	E56	D124, W125 **F128**	None	L262, L263	H289
	2DHD_A [127]	0AK 124_A	G55, E56	Q123, W125, G127, **F128**	N148, A149	L262, L263	H289
	2BFN_A [128]	D2P 1297_A	N38	D108	**I134**	L177, L248	H272, F273
13. Dienelactone hydrolase	1ZJ4_A [95]	SEB 123_A	D36, I37, F38	Y122, L124, G126, **A127**	Y144, Y145, **V147**	F173, V174	H202, S203
14. Carbon-carbon bond hydrolase	2RHW_A [129]	C0E 288_A	G41, G42, G43, A46	N111, A112, M113	**G138**, G139	F239, V240	H265, W266
15. Biotin biosynthesis protein BioH	1M33_A [130]	3OH 300_A	G21, W22, L24	W81, S82, L83	None	L209	H235
	4ETW_A [39]	ZMK 600_B	G21, W22, L24	W81, S82, L83	None	L209	H235
16. Aclacinomycin methylesterase RdmC	1Q0R_A [97]	AKT 600_A	G32, N33	S102, M103, **T106**	L126, G127, **G128**, G129	I250, A251	H276
17. Carboxylesterase/lipase	1TQH_A [131]	4PA 701_A	G24, F25, T26, G27	L93, S94, L95	**P118**	M195, I196	H223, V224
18. Epoxide hydrolase	3G02_A [132]	FMT 408_A	W117	D192	None	W284, L349	No
	3G0I_A [132]	VPR 1_A	W117	D192, I193, **F196**	**L215**	W284, L349	H374
19. Haloperoxidase	1A8U_A [100]	BEZ 295_A	G31, F32	F97, S98, M99	**L125**	T230, L231	H257

(Continued)

Table 2. (Continued)

SCOP family # / SCOP family name	PDB ID Reference	Ligand	Oxyanion zone	Nucleophile zone	Strand β6	Catalytic acid zone	Catalytic base loop
20. Thioesterases	1EXW_A [133]	HDS 430_A	G40, M41	S115, Q116	**Q142**	I235, V236	H289, L290
21. Carboxylesterase/ thioesterase 1	5SYM_A [134]	71Q 301_A	L30	S119, Q120	**W145**, L146	L176, V177	None
22. Ccg1/TafII250-interacting factor B (Cib)	1IMJ_A [103]	SO4 211_A	G40, I41, R42, F43	S111, L112	None	M164	H188, P189, Y191
23. A novel bacterial esterase	2WKW_A [104]	W22 577_A	G70, C71, C72, L73	H205, S206, Q207	**G232**	F145, W262	H298
25. Fungal lipases	5A71_A [135]	IPA 1319_A	T40	S105	**D134**	I189, V190	H224
26. Bacterial lipase	1R50_A [136]	SIL 277_A	G11, I12, G13, G14	H76, S77, M78	**A105**	I135, V136	H156, I157, L160
27. Pancreatic lipase, N-terminal domain	1LPB_B [137]	MUP 901_B	G76, F77, D79	H151, S152, L153	**A178**	F215	H263, L264
28. Hydroxynitrile lyase-like	3C70_A [109]	SCN 1001_A	T11, I12, H14	S80, C81	None	I209, F210	H235, K236
30. Cutinase-like	1G66_A [138]	SO4 210_A	E12, T13	S90, Q91	**P134**	Y177	H187, Q188
33. Acylaminoacid-releasing enzyme, C-terminal domain	4RE5_A [139]	Y3A 601_A	G368, G369, P370, F371	S445, Y446	**V471**	R526, T527	H556
34. Hypothetical esterase YJL068C	3C6B_A [115]	SDP 161_A	G57, L58, C60	H160, M162, G164, **Y165**	F186, A187, P188, **I189**	F243, L248	H276, Y278
37. PHB depolymerase-like	2D81_A [118]	RB3 451_A	C250, L251	A39, S40, **Y43**	None	T123, V124	H155

family #18). The comparison of the ligand-binding sites in each of the three ABH fold families has shown that, regardless of the structure of ligand, the residues that are involved in the coordination of the imidazole ring of the catalytic histidine (Leu246 and Leu198 in SshEstI) consistently interact with the ligand too; the same applies for the second residue of the oxyanion hole that repeatedly forms contacts with the ligand.

To sum up, by comparing the active sites of ligand-bound ABH fold enzymes, we have found that the role of the catalytic structural core is not limited to the coordination of the residues of the catalytic mechanism, but rather, many residues of the conserved structural core also belong to the ligand-binding site. Thus, residues that already have a critical role in the structural integrity of the catalytic mechanism, appear to be involved in the binding of the ligand, with the residues that coordinate the imidazole ring of the catalytic histidine and the second residue of the oxyanion hole being the most common sites of interaction between the conserved structural core and the bound ligand. In the Discussion section, below, we analyze the role of the novel structural elements that are involved in the optimal arrangement of the catalytic triad, and we review their contribution to the conserved geometry of the structural core and the enzymatic activity of ABH fold enzymes.

Discussion

The focal point of this study is the identification of conserved elements that determine the structural arrangement of the catalytic triad in the ABH fold, aiming to complete the description of the catalytic structural core which was initiated in our previous studies [8, 9]. Specifically, we have earlier introduced three conserved and planar structural organizations that

belong to the active site of ABH fold enzymes: the "catalytic acid zone", the "nucleophile zone" and the "oxyanion zone", which coordinate the catalytic acid, nucleophile and the residues of the oxyanion hole respectively, and help to fix the catalytic histidine loop over the β-sheet, placing the catalytic histidine close to the other residues of the catalytic triad. Nonetheless, the identification of the three conserved structural organizations only partially explains how the catalytic residues are properly arranged next to each other, because until now there has been insufficient information about the coordination of the catalytic histidine.

Therefore, in this comprehensive analysis, we have explored the active sites of ABH fold enzymes, looking for structural elements that coordinate the residues of the catalytic triad with respect to each other. Our research has been narrowed down to the areas around the catalytic nucleophile-histidine pair and the catalytic acid-histidine pair, where we have identified several structural elements which participate in the optimal arrangement of the residues of the catalytic mechanism. By comparing ligand-bound ABH structures, we have found that conserved structural elements of the catalytic core also engage in ligand binding. Thus, in this section, we discuss our findings and suggest that the conserved, structural elements at the active site of ABH fold enzymes have versatile roles that extend from the coordination of the catalytic residues and the structural integrity of the catalytic mechanism to the binding of ligands and affecting other properties of the enzymatic activity.

Six conserved interactions coordinate the catalytic histidine next to the catalytic acid and the catalytic nucleophile, and are proven to be critical components for the overall structural stability of the catalytic mechanism

The main concern of this study is the coordination of the catalytic histidine at the active site of ABH fold enzymes. Because the catalytic histidine is located at a flexible loop, it cannot be coordinated by a similar closed structural organization, as in the cases of the catalytic acid, the catalytic nucleophile and the oxyanion hole. Moreover, in a few ABH fold enzymes it has been observed that when the enzyme is inactive, the catalytic histidine is displaced from the catalytic site, but upon ligand binding, the catalytic mechanism is readily re-assembled and the enzyme is again capable of functioning [15–17], which suggests that the flexibility of the histidine loop is also utilized for the regulation of the enzymatic activity. Instead of a closed structural organization, the comparative analysis of active sites from 40 ABH fold enzyme families has shown that the coordination of the catalytic histidine next to the catalytic nucleophile and the catalytic acid is achieved by six conserved interactions from five neighboring residues that coordinate the catalytic histidine, as reviewed below.

Located at the C-terminus of strand β6, at a sharp turn that is suggested to be critical for the position of the residues of the catalytic triad [18–20], residue X_{IV} and residue X_{IV+1} coordinate the catalytic nucleophile-histidine pair. Specifically, residue X_{IV} uses its main-chain oxygen atom to interact with both the catalytic histidine and the catalytic nucleophile, fixing the side chain of the catalytic histidine close to the side chain of the catalytic nucleophile. Residue X_{IV+1} interacts with the main-chain oxygen atom of the catalytic nucleophile, and supports the optimal arrangement of the catalytic nucleophile-histidine pair, through the coordination of the catalytic nucleophile.

In the catalytic acid-histidine pair, it appears that the catalytic acid plays a critical role in the coordination of the catalytic histidine because its side-chain oxygen atoms form two weak hydrogen bonds with the CA and CB atoms of the catalytic histidine. The imidazole ring of the catalytic histidine is further coordinated by nearby residues, usually through two contacts. The first contact is a hydrophobic interaction that takes place between the imidazole ring and residue X_{acid+3} (or in a few cases, with residue X_{acid+2} instead). The second interaction, a CH–π

interaction, usually involves the side chain of residue X_{acid+2} or some other residue that stands opposite to the β-sheet and at interacting distance with the imidazole ring.

The findings of this research provide additional information about the role of the catalytic acid zone. The two weak hydrogen bonds between the catalytic histidine and the catalytic acid make the catalytic acid zone directly responsible for the coordination of the catalytic histidine, in addition to the contribution of the catalytic acid zone to the stabilization of the histidine loop. Moreover, in the general vicinity of the catalytic acid zone, residue X_{acid+2} is noteworthy for its two-fold contribution in the coordination of the catalytic histidine, because it not only coordinates the imidazole ring of the catalytic histidine, but X_{acid+2} is also part of the Asx-motif, which is suggested to aid the correct orientation of the catalytic histidine in the ABH enzymes that have a catalytic aspartic acid after strand β7 [21]. In particular, the Asx-motif occurs at the turn after strand β7 and includes the catalytic aspartic acid, residue X_{acid+2}, and frequently residue X_{acid+3}, which together form a hydrogen-bonding network that connects the side-chain oxygen of the catalytic acid with the main-chain nitrogen atoms of residue X_{acid+2} and residue X_{acid+3}; the same side-chain oxygen of the catalytic acid interacts with the catalytic histidine, and thus, the Asx-motif is thought to help stabilize the catalytic histidine. Remarkably, we have found that residue X_{acid+2} regularly interacts with both residue X_{IV} and residue X_{IV+1}, which indicates that the conserved structural elements that surround the residues of the catalytic triad are joined together in a circular manner.

All things considered, our observations suggest that the catalytic triad is coordinated by an extended network of interwoven contacts among neighboring residues that are located at conserved positions on the ABH fold. Residue X_{IV}, residue X_{IV+1} and residue X_{acid+2} are prime structural elements of the catalytic core that orchestrate the optimal arrangement of the catalytic triad, with the interactions that involve residue X_{IV}, residue X_{IV+1} and residue X_{acid+2} clearly ensuring the structural integrity of the catalytic mechanism in the active site of ABH enzymes.

The conserved structural elements that line the catalytic structural core of ABH fold enzymes are important for the enzymatic function because they are actively involved in ligand binding and affect other properties of the enzymatic activity

With the identification of the conserved structural elements that coordinate the catalytic histidine next to the catalytic acid and the catalytic nucleophile, and combined with the determination of the conserved geometries that surround the catalytic acid, the catalytic nucleophile and the residues that form the oxyanion hole, we suggest that the sum of the conserved structural elements that we have in all three studies make up the conserved catalytic structural core, which is the minimum common structure of the active site of ABH fold enzymes.

The catalytic structural core is located at the interior of the ABH fold proteins and extends from the area around the catalytic acid to the area around the oxyanion hole. The elements that comprise the catalytic structural core are located at conserved positions across the ABH fold, including the C-termini of strand β3-β7, the N-termini of helix αA and αC, the turn after strand β7 and a part of the flexible loop after strand β8. Considering the striking conservation rate of the catalytic structural core in the 40 ABH fold enzyme families, it seems that the "skeleton" of the active site is largely maintained among the ABH fold enzymes, regardless of the catalytic versatility that characterizes the structural family of alpha/beta-Hydrolases.

Based on this observation, we have explored ligand-bound ABH structures to find out how the conserved structural core correlates with the binding site of ABH fold enzymes, where we have verified that several conserved structural residues of the active site interact with the

ligand, and thus, the distinct architecture of the conserved catalytic core also serves ligand binding (Table 2). However, we have observed that ligand binding is also dependent on hydrophobic/aromatic residues that are located before and after the conserved structural residues, such as the residues that precede and follow residue X_{acid+2}, residue X_{IV+2} that follows the dipeptide residue X_{IV}—residue X_{IV+1}, and the residues at the N-terminus of loop$_{\beta3\rightarrow\alpha A}$ that follow the oxyanion zone. Therefore, we perceive that the conserved structural core acts as a supportive framework for residues that form the hydrophobic binding pocket, which are not conserved structural elements. The conserved structural core also acts as a stable infrastructure for other insertions on the ABH fold that are related to the function of the enzyme, such as for the "lids" or "caps" that occur after strand β6 [20, 22–28] and for the insertions at loop$_{\beta3\rightarrow\alpha A}$ that we have reviewed in our previous study [9].

Multiple studies refer to the elements of the conserved structural core and their versatile roles in the enzymatic activity of ABH fold proteins. Residue X_{IV} has previously drawn attention because of its position close to the catalytic triad and its interaction with the catalytic residues in several ABH fold enzymes [29–32]. The low rate of amino-acid conservation at position IV hints that residue X_{IV} could affect the enzymatic activity, given that its side chain has a suitable conformation that does not interfere with the catalytic triad, with amino acids of variable side-chain lengths occurring at position IV, including glutamine [33] and tryptophan [34]. Indeed, residue X_{IV} is suggested to be involved in the optimal configuration of the catalytic triad [32, 35] and the enzymatic activity [36–38], to participate in substrate binding [15, 30, 38–41] and to affect the thermostability [35] of ABH fold enzymes. Site-directed mutagenesis of residue X_{IV} in different ABH fold enzymes has confirmed its significance in the enzymatic activity, resulting in a wide range of effects upon its replacement: from decreased [32, 35–37] and acute loss [38] of enzymatic activity, to improved activity [36, 38, 41] and increased thermostability [35]. These observations are consistent with the high rate of amino-acid variability of residue X_{IV}.

Residue X_{IV+1} has been suggested to be a determinant of the local geometry [6], frequently occupied by small amino acids (glycine and proline in Table 1) that are suitable for limiting the steric clashes within the active site pocket. Residue X_{IV+1} has also been mentioned as part of the hydrophobic binding pocket [39] and the helical domain that occurs after strand β6 [20], while in some cases it can affect the enzymatic activity [42–44]. To our knowledge, there is only one mutational study that refers to residue X_{IV+1}, where its substitution has resulted in nearly complete loss of catalytic activity [45]. The tripeptide residue X_{IV}—residue X_{IV+1}—residue X_{IV+2} retains its amino-acid conservation in some ABH fold enzyme families, and thus, it is suggested that it can be used as an additional sequence identifier of different ABH fold enzyme families [32, 37]. Residue X_{IV+2} is also extensively studied for the formation of the hydrophobic substrate pocket [22, 25, 32, 37–39, 46–48] and its role in the enzymatic function [32, 49, 50].

Residue X_{acid+2}, one of the conserved structural elements that is involved in the coordination of the imidazole ring of the catalytic histidine, is usually a hydrophobic or an aromatic residue located at the entrance of the active site cleft, mostly reviewed for its role in ligand binding [51–56] or the release of products of catalysis [51, 57]. Consequently, the site-directed mutagenesis of residue X_{acid+2} in different ABH enzymes has led to various results, which are consistent with its role in ligand binding, including the compromising [52, 54, 55, 58, 59] or the enhancement [52] of catalytic activity, the alteration of transport tunnels [57, 60], the modification of substrate specificity [53, 55, 56] and the inversion of enantioselectivity [52]. For the remaining residues that coordinate the imidazole ring of the catalytic histidine, including residue X_{acid+3}, we have only found a few mutational studies that have resulted in reduced activity

[58, 61, 62], with a single study highlighting the residue's role in the stability of the enzyme and the catalytic activity rather than in ligand binding [58].

Residue X_{IV} forms conserved interactions with the residues of the catalytic triad in all ABH fold enzymes and thus, can be perceived as the fourth member of a "structural catalytic tetrad"

From a structural point of view, residue X_{IV} undoubtedly is the connecting point of all residues of the acid-base-nucleophile catalytic triad in ABH fold enzymes. Residue X_{IV} is a conserved structural element of the catalytic acid zone that consistently interacts with the catalytic acid when it is located after strand β7, or alternatively, residue X_{IV} is the catalytic acid [8]. Through a contact that is conserved among serine hydrolases, the catalytic histidine also interacts with residue X_{IV} and is speculated to have a functional role in the catalytic mechanism [10]. Here, we have confirmed that residue X_{IV} invariably interacts with the catalytic nucleophile, too. Because of the absolute conservation of the hydrogen-bonding network between residue X_{IV} and the residues of the catalytic triad, we suggest that residue X_{IV} can be viewed as the fourth part of a "structural catalytic tetrad". This idea is not novel: earlier studies have pointed out residue X_{IV} to be part of the catalytic mechanism in ABH fold enzymes, by providing structural support to the members of the catalytic triad [63–65]. Yet, this observation is not unique in ABH fold enzymes either, because residues that are located near catalytic residues are often studied for their structural role and effects on the catalytic mechanism of enzymes from other families, too [66, 67].

The conserved interaction network between residue X_{IV} and the residues of the catalytic triad is facilitated by the favorable side-chain conformation of residue X_{IV}, which does not conflict sterically with the side chains of the catalytic residues under any circumstances. Based on our findings, it is clear that the amino-acid type of residue X_{IV} is not structurally important for the catalytic mechanism itself, but it is the position of residue X_{IV} on the ABH fold that determines its structural role. Thus, we suggest that the position of residue X_{IV} is an equally conserved feature of the catalytic core as those positions that accommodate the catalytic residues. Our claim is further supported when we consider the ABH fold enzymes that have non-canonical catalytic triads [68–73], where the positions of the catalytic residues can be defined more precisely by their spatial arrangement on the catalytic core, rather than their sequence position across the polypeptide chain.

Conclusions

In this study, we have explored the active sites of enzymes from 40 ABH fold enzyme families, aiming to determine the structural basis for the optimal arrangement of the residues of the acid-base-nucleophile catalytic triad. Complementary to the findings of our previous research, we have here identified a set of conserved structural elements that coordinate the catalytic histidine next to the catalytic nucleophile and the catalytic acid, leading to the fine tuning of the catalytic residues. The results of this study prove that all key units of the catalytic mechanism–the catalytic acid, the catalytic histidine, the catalytic nucleophile and the residues of the oxyanion hole–are coordinated by conserved structural elements that altogether comprise the conserved catalytic core of the ABH fold enzymes.

The relationship between structure and function in ABH fold enzymes is also addressed with this research, because we have demonstrated that the function of the catalytically diverse ABH fold enzymes widely relies on the conserved structural framework that surrounds the catalytic mechanism. Indeed, the conserved structural core secures the structural integrity of the catalytic machinery, while the conserved elements that line the active site of ABH fold enzymes

influence the enzymatic activity. In particular, the elements of the conserved structural core participate in ligand binding and are experimentally proven to affect enzymatic properties, such as the substrate specificity, the enantioselectivity, the thermostability and the pH optimum of ABH fold enzymes.

The modification of enzymatic properties is one of the main tasks of protein engineering and the ABH fold enzymes are often selected as targets for tailoring catalysts with improved properties. We expect that our findings can advance the efficacy of protein engineering applications because the conserved structural core offers an ideal template of potential modification sites and thus, we perceive that the conserved elements of the structural core certainly deserve research attention when attempting to customize the catalytic properties of ABH fold enzymes. The usefulness of our results is based on this comprehensive analysis of the active site of ABH fold enzymes that takes into consideration the conserved structural features of the ABH fold common among all ABH fold enzymes, while taking less notice of the individual variations that occur among the different classes of catalysts that belong to the ABH fold structural family.

Finally, the identification of the conserved structural core signifies that the function of all ABH fold enzymes is based on a minimal, but stabile infrastructure, which could explain the widespread occurrence of ABH fold enzymes in nature and their ability to catalyze various reactions on different substrates. However, the alpha/beta-Hydrolases are not the only enzymes with an acid-base-nucleophile catalytic triad and subsequently, the notion of the conserved structural core around the catalytic mechanism should be explored in other classes of enzymes that use an acid-base-nucleophile catalytic triad in order to catalyze reactions (such as trypsins, chymotrypsins, subtilisins and serine proteases) or in other enzymes that have alpha/beta-hydrolases fold structures.

P.S. One of the manuscript reviewers asked us an important question: "whether the weak hydrogen-bonding interactions (3.8 Å and more) do really contribute to protein stability at ambient temperatures?" To answer this question, we analyzed the X-ray diffraction data of three proteins obtained at cryogenic and room temperatures. The analysis results are presented in S1C Table. Two conclusions follow from them:

1. BIOVIA (Accelrys) Discovery Studio [74] enables the reliable inclusion of calculated hydrogen atoms in enzyme structures with resolution ≤ 2.2 Å.

2. The conformational characteristics of weak hydrogen bonds do not change significantly when enzyme structures are compared at cryogenic and room temperatures.

Materials and methods

The representative structures of our dataset are selected based on the categorization of ABH fold families that is provided by the Structural Classification of Proteins (SCOP) database [11]. The SCOP database classifies 41 ABH families, which altogether contain 128 different entries of ABH proteins. We have excluded the single entry from the TTHA1544-like family (SCOP Family #39) because it is not a hydrolase [75]. The remaining 40 ABH enzyme families contain in total 127 entries, from which we have chosen the highest resolution structure to represent each one of the 40 ABH fold enzyme families. Additionally, we have included the two carboxylestarases SshEstI and EstFa_R from the study of Ohara *et al.* [13] that we use as reference structures for our analysis. All protein structures are obtained from Protein Data Bank (PDB) [12].

The results of this study are presented in two tables, with each table containing a different number of entries. Table 1 contains representative structures from the 40 ABH fold enzymes

families plus the carboxylesterase SshEstI (second row); all structures are unligated, except for SshEstI. The conserved interactions that are shown in Table 1 refer to the two contacts that coordinate the catalytic nucleophile-histidine pair (column CA/Nucleophile–O/X$_{IV}$ and column O/Nucleophile–CA/X$_{IV+1}$) and the additional conserved interaction that is located at the catalytic site of ABH fold enzymes (Sc/(Nucleophile+4)–O/X$_{IV+2}$).

Table 2 contains ligand-bound structures from 28 ABH fold enzyme families plus the carboxylesterase SshEstI (second row), while three of the 28 ABH fold families are represented by more than one structures (SCOP families: #12 Haloalkane dehalogenase, #15 Biotin biosynthesis protein BioH, #18 Epoxide hydrolase). The ligand-bound structures of Table 2 correspond to the ligand-free structures of Table 1, and thus, in Table 2 we have omitted the twelve ABH fold families for which we have found no equivalent ligand-bound structures. The columns of Table 2 describe the residues of the conserved structural core that are involved in ligand binding, whereby the residues are distributed in the columns based on their position close to the one of the key units of the catalytic mechanism.

For all structural analyses, such as identification of hydrogen bonds, hydrophobic or other types of weak interactions, we have used the BIOVIA (Accelrys) Discovery Studio [74] (http://accelrys.com/products/collaborativescience/bioviadiscoverystudio/), the Ligand-Protein Contacts software and the Contacts of Structural Units software (LPC; CSU) [76]. We have identified the weak hydrogen bonds from CH–O contacts in structures with at least 2.0 Å resolution based on geometrical criteria given in Derewenda *et al.* [77] and with distances C . . . O $\leq$ 4.1 Å and H . . . O $\leq$ 3.0 Å, and the weak hydrogen bonds from CH–π contacts with distance between 3.4 Å and 6Å [78, 79].

Lastly, for the visualization and analysis of the structural data, we have used BIOVIA (Accelrys) Discovery Studio [74] and Bodil [80]. Figures are drawn with MolScript [81].

Supporting information

S1 Table. Interactions within the catalytic core in ABH fold enzyme families.
(DOCX)

Author Contributions

Conceptualization: Alexander Denesyuk, Polytimi S. Dimitriou, Konstantin Denessiouk.

Data curation: Polytimi S. Dimitriou, Mark S. Johnson, Toru Nakayama.

Formal analysis: Alexander Denesyuk, Polytimi S. Dimitriou.

Funding acquisition: Mark S. Johnson.

Investigation: Polytimi S. Dimitriou, Toru Nakayama, Konstantin Denessiouk.

Methodology: Alexander Denesyuk, Polytimi S. Dimitriou.

Supervision: Alexander Denesyuk, Mark S. Johnson, Toru Nakayama, Konstantin Denessiouk.

Writing – original draft: Polytimi S. Dimitriou, Mark S. Johnson, Konstantin Denessiouk.

Writing – review & editing: Polytimi S. Dimitriou, Mark S. Johnson, Konstantin Denessiouk.

References

1. Nardini M, Dijkstra BW (1999) α/β-Hydrolase fold enzymes: the family keeps growing. Curr Opin Struct Biol 9:732–737. https://doi.org/10.1016/s0959-440x(99)00037-8 PMID: 10607665

2. Mindrebo JT, Nartey CM, Seto Y, Burkart MK, Noel JP (2016) Unveiling the functional diversity of the alpha/beta-hydrolase superfamily in the plant kingdom. Curr Opin Struct Biol 41:233–246. https://doi.org/10.1016/j.sbi.2016.08.005 PMID: 27662376

3. Lenfant N, Hotelier T, Velluet E, Bourne Y, Marchot P, Chatonnet A (2013) ESTHER, the database of the α/β-hydrolase fold superfamily of proteins: tools to explore diversity of functions. Nucleic Acids Res 41:D423–D429. https://doi.org/10.1093/nar/gks1154 PMID: 23193256

4. Jochens H, Hesseler M, Stiba K, Padhi SK, Kazlauskas RJ, Bornscheuer UT (2011) Protein engineering of α/β-hydrolase fold enzymes. ChemBioChem 12:1508–1517. https://doi.org/10.1002/cbic.201000771 PMID: 21506229

5. Rauwerdink A, Kazlauskas RJ (2015) How the same core catalytic machinery catalyzes 17 different reactions: the serine-histidine-aspartate catalytic triad of α/β-hydrolase fold enzymes. ACS Catalysis 5:6153–6176. https://doi.org/10.1021/acscatal.5b01539 PMID: 28580193

6. Ollis DL, Cheah E, Cygler M, Dijkstra B, Frolow F, Franken SM, et al. (1992) The α/β hydrolase fold. Protein Eng 5:197–211. https://doi.org/10.1093/protein/5.3.197 PMID: 1409539

7. Heikinheimo P, Goldman A, Jeffries C, Ollis DL (1999) Of barn owls and bankers: a lush variety of α/β hydrolases. Structure 7:141–146.

8. Dimitriou PS, Denesyuk A, Takahashi S, Yamashita S, Johnson MS, Nakayama T, et al. (2017) Alpha/beta-hydrolases: a unique structural motif coordinates catalytic acid residue in 40 protein fold families. Proteins 85:1845–1855. https://doi.org/10.1002/prot.25338 PMID: 28643343

9. Dimitriou PS, Denesyuk A, Nakayama T, Johnson MS, Denessiouk K (2019) Distinctive structural motifs co-ordinate the catalytic nucleophile and the residues of the oxyanion hole in the alpha/beta-hydrolase fold enzymes. Protein Sci 28:344–364. https://doi.org/10.1002/pro.3527 PMID: 30311984

10. Derewenda ZS, Derewenda U, Kobos PM (1994) (His)C epsilon-H . . .O = C < hydrogen bond in the active sites of serine hydrolases. J Mol Biol 241:83–93. https://doi.org/10.1006/jmbi.1994.1475 PMID: 8051710

11. Murzin AG, Brenner SE, Hubbard T, Chothia C (1995) SCOP: a structural classification of proteins database for the investigation of sequences and structures. J Mol Biol 247:536–540. https://doi.org/10.1006/jmbi.1995.0159 PMID: 7723011

12. Berman HM, Westbrook J, Feng Z, Gilliland G, Bhat TN, Weissig H, et al. (2000) The protein data bank. Nucleic Acids Res 28:235–242. https://doi.org/10.1093/nar/28.1.235 PMID: 10592235

13. Ohara K, Unno H, Hosoya M, Fujino N, Hirooka K, Takahashi S, et al. (2014) Structural insights into the low pH adaptation of a unique carboxylesterase from *Ferroplasma*: altering the pH optima of two carboxylesterases. J Biol Chem 289:24499–24510. https://doi.org/10.1074/jbc.M113.521856 PMID: 25043762

14. Larsen NA, Lin H, Wei R, Fischbach MA, Walsh CT (2006) Structural characterization of enterobactin hydrolase IroE. Biochemistry 45:10184–10190. https://doi.org/10.1021/bi060950i PMID: 16922493

15. McAuley KE, Svendsen A, Patkar SA, Wilson KS (2004) Structure of a feruloyl esterase from *Aspergillus niger*. Acta Crystallogr D Biol Crystallogr. 60:878–887. https://doi.org/10.1107/S0907444904004937 PMID: 15103133

16. Liu P, Ewis HE, Tai PC, Lu CD, Weber IT (2006) Crystal structure of the *Geobacillus stearothermophilus* carboxylesterase Est55 and its activation of prodrug CPT-11. J Mol Biol 367:212–223. https://doi.org/10.1016/j.jmb.2006.12.067 PMID: 17239398

17. Sun Y, Yin S, Feng Y, Li J, Zhou J, Liu C, et al. (2014) Molecular basis of the general base catalysis of an α/β-hydrolase catalytic triad. J Biol Chem 289:15867–15879. https://doi.org/10.1074/jbc.M113.535641 PMID: 24737327

18. Pathak D, Ollis D. (1990) Refined structure of dienelactone hydrolase at 1.8 Å. J Mol Biol 214:497–525. https://doi.org/10.1016/0022-2836(90)90196-s PMID: 2380986

19. Robinson A, Edwards KJ, Carr PD, Barton JD, Ewart GD, Ollis DL (2000) Structure of the C123S mutant of dienelactone hydrolase (DLH) bound with the PMS moiety of the protease inhibitor phenylmethylsulfonyl fluoride (PMSF). Acta Crystallogr D Biol Crystallogr. 56:1376–1384. https://doi.org/10.1107/s0907444900010647 PMID: 11053834

20. Rigolet P, Mechin I, Delage MM, Chich JF. (2002) The structural basis for catalysis and specificity of the X-prolyl dipeptidyl aminopeptidase from *Lactococcus lactis*. Structure 10:1383–1394. https://doi.org/10.1016/s0969-2126(02)00851-1 PMID: 12377124

21. Wan WY, Milner-White EJ (1999) A natural grouping of motifs with an aspartate or asparagine residue forming two hydrogen bonds to residues ahead in sequence: their occurrence at alpha-helical N termini and in other situations. J Mol Biol 286:1633–1649. https://doi.org/10.1006/jmbi.1999.2552 PMID: 10064720

22. De Simone G, Menchise V, Manco G, Mandrich L, Sorrentino N, Lang D, et al. (2001) The crystal structure of a hyper-thermophilic carboxylesterase from the archaeon *Archaeoglobus fulgidus*. J Mol Biol 314:507–518. https://doi.org/10.1006/jmbi.2001.5152 PMID: 11846563

23. Johnston JM, Jiang M, Guo Z, Baker EN (2010) Structural and functional analysis of Rv0554 from *Mycobacterium tuberculosis*: testing a putative role in menaquinone biosynthesis. Acta Crystallogr D Biol Crystallogr 66:909–917. https://doi.org/10.1107/S0907444910025771 PMID: 20693690

24. Lai KK, Stogios PJ, Vu C, Xu X, Cui H, Molloy S, et al. (2011) An inserted α/β sub-domain shapes the catalytic pocket of *Lactobacillus johnsonii* cinnamoyl esterase. PLoS One 6:e23269. https://doi.org/10.1371/journal.pone.0023269 PMID: 21876742

25. Rengachari S, Bezerra GA, Riegler-Berket L, Gruber CC, Sturm C, Taschler U, et al. (2012) The structure of monoacylglycerol lipase from *Bacillus* sp. H257 reveals unexpected conservation of the cap architecture between bacterial and human enzymes. Biochim Biophys Acta 1821:1012–1021. https://doi.org/10.1016/j.bbalip.2012.04.006 PMID: 22561231

26. Alvarez Y, Esteban-Torres M, Cortés-Cabrera A, Gago F, Acebrón I, Benavente R, et al. (2014) Esterase LpEst1 from *Lactobacillus plantarum*: a novel and atypical member of the αβ hydrolase superfamily of enzymes. PLoS One 9:e92257. https://doi.org/10.1371/journal.pone.0092257 PMID: 24663330

27. Perz V, Baumschlager A, Bleymaier K, Zitzenbacher S, Hromic A, Steinkellner G, et al. (2016) Hydrolysis of synthetic polyesters by *Clostridium botulinum* esterases. Biotechnol Bioeng 113:1024–1034. https://doi.org/10.1002/bit.25874 PMID: 26524601

28. Gruninger RJ, Cote C, McAllister TA, Abbott DW (2016) Contributions of a unique β-clamp to substrate recognition illuminates the molecular basis of exolysis in ferulic acid esterases. Biochem J 473:839–849. https://doi.org/10.1042/BJ20151153 PMID: 27026397

29. Elmi F, Lee HT, Huang JY, Hsieh YC, Wang YL, Chen YJ, et al. (2002) Stereoselective Esterase from *Pseudomonas putida* IFO12996 Reveals α/β Hydrolase Folds for D-β-Acetylthioisobutyric Acid Synthesis. J Bacteriol 187:8470–8476.

30. Bythell-Douglas R, Waters MT, Scaffidi A, Flematti GR, Smith SM, Bond CS (2013) The structure of the karrikin-insensitive protein (KAI2) in *Arabidopsis thaliana*. PLoS One 8:e54758. https://doi.org/10.1371/journal.pone.0054758 PMID: 23349965

31. Rozeboom HJ, Godinho LF, Nardini M, Quax WJ, Dijkstra BW (2014) Crystal structures of two *Bacillus* carboxylesterases with different enantioselectivities. Biochim Biophys Acta 1844:567–575. https://doi.org/10.1016/j.bbapap.2014.01.003 PMID: 24418394

32. Payne K, Sun Q, Sacchettini J, Hatfull GF (2009) Mycobacteriophage Lysin B is a novel mycolylarabinogalactan esterase. Mol Microbiol 73:367–381. https://doi.org/10.1111/j.1365-2958.2009.06775.x PMID: 19555454

33. McKary MG, Abendroth J, Edwards TE, Johnson RJ (2016) Structural Basis for the Strict Substrate Selectivity of the *Mycobacterial* Hydrolase LipW. Biochemistry 55:7099–7111. https://doi.org/10.1021/acs.biochem.6b01057 PMID: 27936614

34. Dou S, Kong XD, Ma BD, Chen Q, Zhang J, Zhou J, et al. (2014) Crystal structures of *Pseudomonas putida* esterase reveal the functional role of residues 187 and 287 in substrate binding and chiral recognition. Biochem Biophys Res Commun 446:1145–1150. https://doi.org/10.1016/j.bbrc.2014.03.072 PMID: 24680822

35. Truongvan N, Chung HS, Jang SH, Lee C (2016) Conserved tyrosine 182 residue in hyperthermophilic esterase EstE1 plays a critical role in stabilizing the active site. Extremophiles 20:187–193. https://doi.org/10.1007/s00792-016-0812-3 PMID: 26838013

36. Lemak S, Tchigvintsev A, Petit P, Flick R, Singer AU, Brown G, et al. (2012) Structure and activity of the cold-active and anion-activated carboxyl esterase OLEI01171 from the oil-degrading marine bacterium *Oleispira antarctica*. Biochem J 445:193–203. https://doi.org/10.1042/BJ20112113 PMID: 22519667

37. Ren B, Wu M, Wang Q, Peng X, Wen H, McKinstry WJ, et al. (2013) Crystal structure of tannase from *Lactobacillus plantarum*. J Mol Biol. 425:2737–2751. https://doi.org/10.1016/j.jmb.2013.04.032 PMID: 23648840

38. Yadav P, Goyal VD, Gaur NK, Kumar A, Gokhale SM, Jamdar SN, et al. (2019) Carboxypeptidase in prolyl oligopeptidase family: unique enzyme activation and substrate-screening mechanisms. J Biol Chem 294:89–100. https://doi.org/10.1074/jbc.RA118.004254 PMID: 30409909

39. Agarwal V, Lin S, Lukk T, Nair SK, Cronan JE (2012) Structure of the enzyme-acyl carrier protein (ACP) substrate gatekeeper complex required for biotin synthesis. Proc Natl Acad Sci U S A 109:17406–17411. https://doi.org/10.1073/pnas.1207028109 PMID: 23045647

40. Fu J, Leiros HK, de Pascale D, Johnson KA, Blencke HM, Landfald B (2013) Functional and structural studies of a novel cold-adapted esterase from an Arctic intertidal metagenomic library. Appl Microbiol Biotechnol 97:3965–3978. https://doi.org/10.1007/s00253-012-4276-9 PMID: 22832985

41. Porter JL, Boon PL, Murray TP, Huber T, Collyer CA, Ollis DL (2015) Directed evolution of new and improved enzyme functions using an evolutionary intermediate and multidirectional search. ACS Chem Biol 10:611–621. https://doi.org/10.1021/cb500809f PMID: 25419863

42. Harel M, Kryger G, Rosenberry TL, Mallender WD, Lewis T, Fletcher RJ, et al. (2000) Three-dimensional structures of *Drosophila melanogaster* acetylcholinesterase and of its complexes with two potent inhibitors. Protein Sci 9:1063–1072. https://doi.org/10.1110/ps.9.6.1063 PMID: 10892800

43. Boublik Y, Saint-Aguet P, Lougarre A, Arnaud M, Villatte F, Estrada-Mondaca S, et al. (2002) Acetylcholinesterase engineering for detection of insecticide residues. Protein Eng 15:43–50. https://doi.org/10.1093/protein/15.1.43 PMID: 11842237

44. Fournier D (2005) Mutations of acetylcholinesterase which confer insecticide resistance in insect populations. Chem Biol Interact 157–158:257–261. https://doi.org/10.1016/j.cbi.2005.10.040 PMID: 16274684

45. Rathi PC, Fulton A, Jaeger KE, Gohlke H (2016) Application of rigidity theory to the thermostabilization of Lipase A from *Bacillus subtilis*. PLoS Comput Biol 12:e1004754. https://doi.org/10.1371/journal.pcbi.1004754 PMID: 27003415

46. Nakajima Y, Ito K, Sakata M, Xu Y, Nakashima K, Matsubara F, et al. (2006) Unusual extra space at the active site and high activity for acetylated hydroxyproline of prolyl aminopeptidase from *Serratia marcescens*. J Bacteriol 188:1599–1606. https://doi.org/10.1128/JB.188.4.1599-1606.2006 PMID: 16452443

47. Kitadokoro K, Thumarat U, Nakamura R, Nishimura K, Karatani H, Suzuki H, et al. (2012) Crystal structure of cutinase Est119 from *Thermobida alba* AHK119 that can degrade modified polyethylene terephthalate at 1.76 Å resolution. Polym Degrad Stab 97:771–775.

48. Alcaide M, Tornés J, Stogios PJ, Xu X, Gertler C, Di Leo R, et al. (2013) Single residues dictate the co-evolution of dual esterases: MCP hydrolases from the α/β hydrolase family. Biochem J 454:157–166. https://doi.org/10.1042/BJ20130552 PMID: 23750508

49. Skoczinski P, Volkenborn K, Fulton A, Bhadauriya A, Nutschel C, Gohlke H, et al. (2017) Contribution of single amino acid and codon substitutions to the production and secretion of a lipase by *Bacillus subtilis*. Microb Cell Fact 16:160. https://doi.org/10.1186/s12934-017-0772-z PMID: 28946879

50. Austin HP, Allen MD, Donohoe BS, Rorrer NA, Kearns FL, Silveira RL, et al. (2018) Characterization and engineering of a plastic-degrading aromatic polyesterase. Proc Natl Acad Sci USA 115:E4350–E4357. https://doi.org/10.1073/pnas.1718804115 PMID: 29666242

51. Fülöp V, Szeltner Z, Renner V, Polgár L (2001) Structures of prolyl oligopeptidase substrate/inhibitor complexes. Use of inhibitor binding for titration of the catalytic histidine residue. J Biol Chem 276:1262–1266. https://doi.org/10.1074/jbc.M007003200 PMID: 11031266

52. Bordes F, Cambon E, Dossat-Létisse V, André I, Croux C, Nicaud JM, et al. (2009) Improvement of *Yarrowia lipolytica* lipase enantioselectivity by using mutagenesis targeted to the substrate binding site. Chembiochem 10:1705–1713. https://doi.org/10.1002/cbic.200900215 PMID: 19504508

53. Bastard K, Perret A, Mariage A, Bessonnet T, Pinet-Turpault A, Petit JL, et al. (2017) Parallel evolution of non-homologous isofunctional enzymes in methionine biosynthesis. Nat Chem Biol 13:858–866. https://doi.org/10.1038/nchembio.2397 PMID: 28581482

54. Czekster CM, Ludewig H, McMahon SA, Naismith JH (2017) Characterization of a dual function macrocyclase enables design and use of efficient macrocyclization substrates. Nat Commun 8:1045. https://doi.org/10.1038/s41467-017-00862-4 PMID: 29051530

55. Bååth JA, Mazurkewich S, Poulsen JCN, Olsson L, Leggio LL, Larsbrink J (2019) Structure–function analyses reveal that a glucuronoyl esterase from *Teredinibacter turnerae* interacts with carbohydrates and aromatic compounds. J Biol Chem 294: 6635–6644. https://doi.org/10.1074/jbc.RA119.007831 PMID: 30814248

56. Kitadokoro K, Kakara M, Matsui S, Osokoshi R, Thumarat U, Kawai F, et al. (2019) Structural insights into the unique polylactate-degrading mechanism of *Thermobifida alba* cutinase. FEBS J 286:2087–2098. https://doi.org/10.1111/febs.14781 PMID: 30761732

57. Klvana M, Pavlova M, Koudelakova T, Chaloupkova R, Dvorak P, Prokop Z, et al. (2009) Pathways and mechanisms for product release in the engineered haloalkane dehalogenases explored using classical and random acceleration molecular dynamics simulations. J Mol Biol 392:1339–1356. https://doi.org/10.1016/j.jmb.2009.06.076 PMID: 19577578

58. Turner JM, Larsen NA, Basran A, Barbas CF, Bruce NC, Wilson IA, et al. (2002) Biochemical characterization and structural analysis of a highly proficient cocaine esterase. Biochemistry 41:12297–12307. https://doi.org/10.1021/bi026131p PMID: 12369817

59. Joo S, Cho IJ, Seo H, Son HF, Sagong HY, Shin TJ, et al. (2018) Structural insight into molecular mechanism of poly(ethylene terephthalate) degradation. Nat Commun 9:382. https://doi.org/10.1038/s41467-018-02881-1 PMID: 29374183

60. Brezovsky J, Babkova P, Degtjarik O, Fortova A, Gora A, Iermak I, et al. (2016) Engineering a de novo transport tunnel. ACS Catal 6:7597–7610.

61. Naffin-Olivos JL, Daab A, White A, Goldfarb NE, Milne AC, Liu D, et al. (2017) Structure determination of *Mycobacterium tuberculosis* serine protease Hip1 (Rv2224c). Biochemistry 56:2304–2314. https://doi.org/10.1021/acs.biochem.6b01066 PMID: 28346784

62. Palm GJ, Reisky L, Böttcher D, Müller H, Michels EAP, Walczak MC, et al. (2019) Structure of the plastic-degrading *Ideonella sakaiensis* MHETase bound to a substrate. Nat Commun 10:1717. https://doi.org/10.1038/s41467-019-09326-3 PMID: 30979881

63. Liao DI, Breddam K, Sweet RM, Bullock T, Remington SJ (1992) Refined atomic model of wheat serine carboxypeptidase II at 2.2 Å resolution. Biochemistry 31:9796–9812. https://doi.org/10.1021/bi00155a037 PMID: 1390755

64. Park SY, Lee SH, Lee J, Nishi K, Kim YS, Jung CH, et al. (2008) High-resolution structure of ybfF from *Escherichia coli* K12: a unique substrate-binding crevice generated by domain arrangement. J Mol Biol 376:1426–1437. https://doi.org/10.1016/j.jmb.2007.12.062 PMID: 18215690

65. Sherlin D, Anishetty S (2015) Mechanistic insights from molecular dynamic simulation of Rv0045c esterase in *Mycobacterium tuberculosis*. J Mol Model 21:90. https://doi.org/10.1007/s00894-015-2630-4 PMID: 25783994

66. Wallace AC, Laskowski RA, Thornton JM (1996) Derivation of 3D coordinate templates for searching structural databases: application to Ser-His-Asp catalytic triads in the serine proteinases and lipases. *Protein Sci* 5:1001–1013. https://doi.org/10.1002/pro.5560050603 PMID: 8762132

67. Krem MM, Di Cera E (2001) Molecular markers of serine protease evolution. EMBO J 20:3036–3045. https://doi.org/10.1093/emboj/20.12.3036 PMID: 11406580

68. Oakley AJ, Klvana M, Otyepka M, Nagata Y, Wilce MC, Damborsky J (2004) Crystal structure of haloalkane dehalogenase LinB from *Sphingomonas paucimobilis* UT26 at 0.95 Å resolution: dynamics of catalytic residues. Biochemistry 43:870–878. https://doi.org/10.1021/bi034748g PMID: 14744129

69. Bourne PC, Isupov MN, Littlechild JA (2000) The atomic-resolution structure of a novel bacterial esterase. Structure 8:143–151. https://doi.org/10.1016/s0969-2126(00)00090-3 PMID: 10673440

70. Roussel A, Yang Y, Ferrato F, Verger R, Cambillau C, Lowe M (1998) Structure and activity of rat pancreatic lipase-related protein 2. J Biol Chem 273:32121–32128. https://doi.org/10.1074/jbc.273.48.32121 PMID: 9822688

71. Bruner SD, Weber T, Kohli RM, Schwarzer D, Marahiel MA, Walsh CT, et al. (2002) Structural basis for the cyclization of the lipopeptide antibiotic surfactin by the thioesterase domain SrfTE. Structure 10:301–310. https://doi.org/10.1016/s0969-2126(02)00716-5 PMID: 12005429

72. Auldridge ME, Guo Y, Austin MB, Ramsey J, Fridman E, Pichersky E, et al. (2012) Emergent decarboxylase activity and attenuation of α/β-hydrolase activity during the evolution of methylketone biosynthesis in tomato. Plant Cell 24:1596–1607. https://doi.org/10.1105/tpc.111.093997 PMID: 22523203

73. Knapik AA, Petkowski JJ, Otwinowski Z, Cymborowski MT, Cooper DR, Majorek KA, et al. (2012) A multi-faceted analysis of RutD reveals a novel family of α/β hydrolases. Proteins 80:2359–2368. https://doi.org/10.1002/prot.24122 PMID: 22641504

74. Discovery Studio Modeling Environment, Release 2017, San Diego: Dassault Systèmes; 2016.

75. Xie Y, Takemoto C, Kishishita S, UchikuboKamo T, Murayama K, Chen L, et al. (2007) Structure of the minimized alpha/beta-hydrolase fold protein from *Thermus thermophilus* HB8. Acta Crystallogr F 63:993–997.

76. Sobolev V, Sorokine A, Prilusky J, Abola EE, Edelman M (1999) Automated analysis of interatomic contacts in proteins. Bioinformatics 15:327–332. https://doi.org/10.1093/bioinformatics/15.4.327 PMID: 10320401

77. Derewenda ZS, Lee L, Derewenda U (1995) The occurrence of CH . . .O hydrogen bonds in proteins. J Mol Biol 252:248–262. https://doi.org/10.1006/jmbi.1995.0492 PMID: 7674305

78. Brandl M, Weiss MS, Jabs A, Sühnel J, Hilgenfeld R (2001) C-H . . .pi-interactions in proteins. J Mol Biol 307:357–377. https://doi.org/10.1006/jmbi.2000.4473 PMID: 11243825

79. Nishio M, Umezawa Y, Fantini J, Weiss MS, Chakrabarti P (2014) CH-π hydrogen bonds in biological macromolecules. Phys Chem Chem Phys 16:12648–12683. https://doi.org/10.1039/c4cp00099d PMID: 24836323

80. Lehtonen JV, Still DJ, Rantanen VV, Ekholm J, Björklund D, Iftikhar Z, et al. (2004) BODIL: a molecular modeling environment for structure-function analysis and drug design. J Comput Aided Mol Des 18:401–419. https://doi.org/10.1007/s10822-004-3752-4 PMID: 15663001

81. Kraulis PJ (1991) MOLSCRIPT: a program to produce both detailed and schematic plots of protein structures. J Appl Cryst 24:946–950.

82. Spiller B, Gershenson A, Arnold FH, Stevens RC (1999) A structural view of evolutionary divergence. Proc Natl Acad Sci U S A 96:12305–12310. https://doi.org/10.1073/pnas.96.22.12305 PMID: 10535917

83. Zhu X, Larsen NA, Basran A, Bruce NC, Wilson IA (2003) Observation of an arsenic adduct in an acetyl esterase crystal structure. J Biol Chem 278:2008–2014. https://doi.org/10.1074/jbc.M210103200 PMID: 12421810

84. Ronning DR, Klabunde T, Besra GS, Vissa VD, Belisle JT, Sacchettini JC (2000) Crystal structure of the secreted form of antigen 85C reveals potential targets for mycobacterial drugs and vaccines. Nat Struct Biol 7:141–146. https://doi.org/10.1038/72413 PMID: 10655617

85. Murayama K, Shirouzu M, Terada T, Kuramitsu S, Yokoyama S (2005) Crystal structure of TT1662 from *Thermus thermophilus* HB8: a member of the alpha/beta hydrolase fold enzymes. Proteins 58:982–984. https://doi.org/10.1002/prot.20361 PMID: 15648092

86. Narasimhan D, Collins GT, Nance MR, Nichols J, Edwald E, Chan J, et al. (2011) Subunit stabilization and polyethylene glycolation of cocaine esterase improves *in vivo* residence time. Mol Pharmacol 80:1056–1065. https://doi.org/10.1124/mol.111.074997 PMID: 21890748

87. Szeltner Z, Rea D, Renner V, Fulop V, Polgar L (2002) Electrostatic effects and binding determinants in the catalysis of prolyl oligopeptidase. Site specific mutagenesis at the oxyanion binding site. J Biol Chem 277:42613–42622. https://doi.org/10.1074/jbc.M208043200 PMID: 12202494

88. Engel M, Hoffmann T, Wagner L, Wermann M, Heiser U, Kiefersauer R, et al. (2003) The crystal structure of dipeptidyl peptidase IV (CD26) reveals its functional regulation and enzymatic mechanism. Proc Natl Acad Sci U S A 100:5063–5068. https://doi.org/10.1073/pnas.0230620100 PMID: 12690074

89. Liao DI, Breddam K, Sweet RM, Bullock T, Remington SJ (1992) Refined atomic model of wheat serine carboxypeptidase II at 2.2 Å resolution. Biochemistry 31:9796–9812. https://doi.org/10.1021/bi00155a037 PMID: 1390755

90. Roussel A, Canaan S, Egloff MP, Rivière M, Dupuis L, Verger R, et al. (1999) Crystal structure of human gastric lipase and model of lysosomal acid lipase, two lipolytic enzymes of medical interest. J Biol Chem 274:16995–17002. https://doi.org/10.1074/jbc.274.24.16995 PMID: 10358049

91. Goettig P, Groll M, Kim JS, Huber R, Brandstetter H (2002) Structures of the tricorn-interacting aminopeptidase F1 with different ligands explain its catalytic mechanism. EMBO J 21:5343–5352. https://doi.org/10.1093/emboj/cdf552 PMID: 12374735

92. Zhang R, Koroleva O, Collert F, Joachimiak A, Midwest Center for Structural Genomics. 1.5 Å crystal structure of the cephalosporin C deacetylase.

93. Ridder IS, Rozeboom HJ, Dijkstra BW (1999) Haloalkane dehalogenase from *Xanthobacter autotrophicus* GJ10 refined at 1.15 A resolution. Acta Crystallogr D Biol Crystallogr 55:1273–1290. https://doi.org/10.1107/s090744499900534x PMID: 10393294

94. Oakley AJ, Klvana M, Otyepka M, Nagata Y, Wilce MC, Damborsky J (2004) Crystal structure of haloalkane dehalogenase LinB from *Sphingomonas paucimobilis* UT26 at 0.95 Å resolution: dynamics of catalytic residues. Biochemistry 43:870–878. https://doi.org/10.1021/bi034748g PMID: 14744129

95. Kim HK, Liu JW, Carr PD, Ollis DL (2005) Following directed evolution with crystallography: structural changes observed in changing the substrate specificity of dienelactone hydrolase. Acta Crystallogr D Biol Crystallogr 61:920–931. https://doi.org/10.1107/S0907444905009042 PMID: 15983415

96. Horsman GP, Ke J, Dai S, Seah SY, Bolin JT, Eltis LD (2006) Kinetic and structural insight into the mechanism of BphD, a C-C bond hydrolase from the biphenyl degradation pathway. Biochemistry 45:11071–11086. https://doi.org/10.1021/bi0611098 PMID: 16964968

97. Jansson A, Niemi J, Mantsala P, Schneider G (2003) Crystal structure of aclacinomycin methylesterase with bound product analogues: implications for anthracycline recognition and mechanism. J Biol Chem 278:39006–39013. https://doi.org/10.1074/jbc.M304008200 PMID: 12878604

98. Seetharaman J, Lew S, Wang D, Kohan E, Patel D, Whitehead T, et al. Northeast Structural Genomics Consortium. Crystal Structure of Engineered Protein. Northeast Structural Genomics Consortium Target OR94.

99. Zou J, Hallberg BM, Bergfors T, Oesch F, Arand M, Mowbray SL, et al. (2000) Structure of *Aspergillus niger* epoxide hydrolase at 1.8 Å resolution: implications for the structure and function of the mammalian microsomal class of epoxide hydrolases. Structure 8:111–122. https://doi.org/10.1016/s0969-2126(00)00087-3 PMID: 10673439

100. Hofmann B, Tolzer S, Pelletier I, Altenbuchner J, van Pee KH, Hecht HJ (1998) Structural investigation of the cofactor-free chloroperoxidases. J Mol Biol 279:889–900. https://doi.org/10.1006/jmbi.1998.1802 PMID: 9642069

101. Bellizzi JJ III, Widom J, Kemp C, Lu JY, Das AK, Hofmann SL, et al. (2000) The crystal structure of palmitoyl protein thioesterase 1 and the molecular basis of infantile neuronal ceroid lipofuscinosis. Proc Natl Acad Sci U S A 97:4573–4578. https://doi.org/10.1073/pnas.080508097 PMID: 10781062

102. Devedjiev Y, Dauter Z, Kuznetsov SR, Jones TL, Derewenda ZS (2000) Crystal structure of the human acyl protein thioesterase I from a single X-ray data set to 1.5 Å. Structure 8:1137–1146. https://doi.org/10.1016/s0969-2126(00)00529-3 PMID: 11080636

103. Padmanabhan B, Kuzuhara T, Adachi N, Horikoshi M (2004) The crystal structure of CCG1/TAF(II) 250-interacting factor B (CIB). J Biol Chem 279:9615–9624. https://doi.org/10.1074/jbc.M312165200 PMID: 14672934

104. Bourne PC, Isupov MN, Littlechild JA (2000) The atomic-resolution structure of a novel bacterial esterase. Structure 8:143–151. https://doi.org/10.1016/s0969-2126(00)00090-3 PMID: 10673440

105. Wei Y, Swenson L, Castro C, Derewenda U, Minor W, Arai H, et al. (1998) Structure of a microbial homologue of mammalian platelet-activating factor acetylhydrolases: *Streptomyces exfoliatus* lipase at 1.9 Å resolution. Structure 6:511–519. https://doi.org/10.1016/s0969-2126(98)00052-5 PMID: 9562561

106. Uppenberg J, Hansen MT, Patkar S, Jones TA (1994) The sequence, crystal structure determination and refinement of two crystal forms of lipase B from *Candida antarctica*. Structure 2:293–308. https://doi.org/10.1016/s0969-2126(00)00031-9 PMID: 8087556

107. Kawasaki K, Kondo H, Suzuki M, Ohgiya S, Tsuda S (2002) Alternate conformations observed in catalytic serine of *Bacillus subtilis* lipase determined at 1.3 Å resolution. Acta Crystallogr D Biol Crystallogr 58:1168–1174. https://doi.org/10.1107/s090744490200714x PMID: 12077437

108. Roussel A, Yang Y, Ferrato F, Verger R, Cambillau C, Lowe M (1998) Structure and activity of rat pancreatic lipase-related protein 2. J Biol Chem 273:32121–32128. https://doi.org/10.1074/jbc.273.48.32121 PMID: 9822688

109. Schmidt A, Gruber K, Kratky C, Lamzin VS (2008) Atomic resolution crystal structures and quantum chemistry meet to reveal subtleties of hydroxynitrile lyase catalysis. J Biol Chem 283:21827–21836. https://doi.org/10.1074/jbc.M801056200 PMID: 18524775

110. Bruner SD, Weber T, Kohli RM, Schwarzer D, Marahiel MA, Walsh CT, et al. (2002) Structural basis for the cyclization of the lipopeptide antibiotic surfactin by the thioesterase domain SrfTE. Structure 10:301–310. https://doi.org/10.1016/s0969-2126(02)00716-5 PMID: 12005429

111. Ghosh D, Erman M, Sawicki M, Lala P, Weeks DR, Li N, et al. (1999) Determination of a protein structure by iodination: the structure of iodinated acetylxylan esterase. Acta Crystallogr D Biol Crystallogr 55:779–784. https://doi.org/10.1107/s0907444999000244 PMID: 10089308

112. Janda IK, Devedjiev Y, Cooper DR, Chruszcz M, Derewenda U, Gabrys A, et al. (2004) Harvesting the high-hanging fruit: the structure of the YdeN gene product from *Bacillus subtilis* at 1.8 angstroms resolution. Acta Crystallogr D Biol Crystallogr 60:1101–1107. https://doi.org/10.1107/S0907444904007188 PMID: 15159570

113. Arndt JW, Schwarzenbacher R, Page R, Abdubek P, Ambing E, Biorac T, et al. (2005) Crystal structure of an alpha/beta serine hydrolase (YDR428C) from *Saccharomyces cerevisiae* at 1.85 Å resolution. Proteins 58:755–758. https://doi.org/10.1002/prot.20336 PMID: 15624212

114. Bartlam M, Wang G, Yang H, Gao R, Zhao X, Xie G, et al. (2004) Crystal structure of an acylpeptide hydrolase/esterase from *Aeropyrum pernix* K1. Structure 12:1481–1488. https://doi.org/10.1016/j.str.2004.05.019 PMID: 15296741

115. Legler PM, Kumaran D, Swaminathan S, Studier FW, Millard CB (2008) Structural characterization and reversal of the natural organophosphate resistance of a D-type esterase, *Saccharomyces cerevisiae* S-formyl-glutathione hydrolase. Biochemistry 47:9592–9601. https://doi.org/10.1021/bi8010016 PMID: 18707125

116. Gorman J, Shapiro L, Burley SK, Midwest Center for Structural Genomics. Structural Genomics target NYSGRCT920 related to A/B-hydrolase fold.

117. Osipiuk J, Xu X, Zheng H, Savchenko A, Edwards A, Joachimiak A, Midwest Center for Structural Genomics. Crystal structure of hypothetical protein Atu1826, a putative alpha/beta hydrolase from *Agrobacterium tumefaciens*.

118. Hisano T, Kasuya K, Tezuka Y, Ishii N, Kobayashi T, Shiraki M, et al. (2006) The crystal structure of polyhydroxybutyrate depolymerase from *Penicillium funiculosum* provides insights into the recognition and degradation of biopolyesters. J Mol Biol 356:993–1004. https://doi.org/10.1016/j.jmb.2005.12.028 PMID: 16405909

119. Mirza IA, Nazi I, Korczynska M, Wright GD, Berghuis AM (2005) Crystal structure of homoserine trans-acetylase from *Haemophilus influenzae* reveals a new family of alpha/beta-hydrolases. Biochemistry 44:15768–15773. https://doi.org/10.1021/bi051951y PMID: 16313180

120. Schleberger C, Sachelaru P, Brandsch R, Schulz GE (2007) Structure and action of a C-C bond cleaving alpha/beta-hydrolase involved in nicotine degradation. J Mol Biol 367:409–418. https://doi.org/10.1016/j.jmb.2006.12.068 PMID: 17275835

121. Narasimhan D, Nance MR, Gao D, Ko MC, Macdonald J, Tamburi P, et al. (2010) Structural analysis of thermostabilizing mutations of cocaine esterase. Protein Eng Des Sel 23:537–547. https://doi.org/10.1093/protein/gzq025 PMID: 20436035

122. Racys DT, Rea D, Fülöp V, Wills M. (2010) Inhibition of prolyl oligopeptidase with a synthetic unnatural dipeptide. Bioorg Med Chem 1813:4775–4782.

123. Engel M, Hoffmann T, Manhart S, Heiser U, Chambre S, Huber R, et al. (2006) Rigidity and flexibility of dipeptidyl peptidase IV: crystal structures of and docking experiments with DPIV. J Mol Biol 355:768–783. https://doi.org/10.1016/j.jmb.2005.11.014 PMID: 16330047

124. Kanamaru S, Ishiwata Y, Suzuki T, Rossmann MG, Arisaka F (2005) Control of bacteriophage T4 tail lysozyme activity during the infection process. J Mol Biol 346:1013–1020. https://doi.org/10.1016/j.jmb.2004.12.042 PMID: 15701513

125. Vincent F, Charnock SJ, Verschueren KH, Turkenburg JP, Scott DJ, Offen WA, et al. (2003) Multifunctional xylooligosaccharide/cephalosporin C deacetylase revealed by the hexameric structure of the *Bacillus subtilis* enzyme at 1.9 Å resolution. J Mol Biol 330:593–606. https://doi.org/10.1016/s0022-2836(03)00632-6 PMID: 12842474

126. Krooshof GH, Ridder IS, Tepper AW, Vos GJ, Rozeboom HJ, Kalk KH, et al. (1998) Kinetic analysis and X-ray structure of haloalkane dehalogenase with a modified halide-binding site. Biochemistry 37:15013–15023. https://doi.org/10.1021/bi9815187 PMID: 9790663

127. Verschueren KH, Seljée F, Rozeboom HJ, Kalk KH, Dijkstra BW (1993) Crystallographic analysis of the catalytic mechanism of haloalkane dehalogenase. Nature 363:693–698. https://doi.org/10.1038/363693a0 PMID: 8515812

128. Monincová M, Prokop Z, Vévodová J, Nagata Y, Damborsky J. (2007) Weak activity of haloalkane dehalogenase LinB with 1,2,3-trichloropropane revealed by X-Ray crystallography and microcalorimetry. Appl Environ Microbiol 73:2005–2008. https://doi.org/10.1128/AEM.02416-06 PMID: 17259360

129. Bhowmik S, Horsman GP, Bolin JT, Eltis LD (2007) The molecular basis for inhibition of BphD, a C-C bond hydrolase involved in polychlorinated biphenyls degradation: large 3-substituents prevent tautomerization. J Biol Chem 282:36377–36385. https://doi.org/10.1074/jbc.M707035200 PMID: 17932031

130. Sanishvili R, Yakunin AF, Laskowski RA, Skarina T, Evdokimova E, Doherty-Kirby A, et al. (2003) Integrating structure, bioinformatics, and enzymology to discover function: BioH, a new carboxylesterase from *Escherichia coli*. J Biol Chem 278:26039–26045. https://doi.org/10.1074/jbc.M303867200 PMID: 12732651

131. Liu P, Wang YF, Ewis HE, Abdelal AT, Lu CD, Harrison RW, et al. (2004) Covalent reaction intermediate revealed in crystal structure of the *Geobacillus stearothermophilus* carboxylesterase Est30. J Mol Biol 342:551–561. https://doi.org/10.1016/j.jmb.2004.06.069 PMID: 15327954

132. Reetz MT, Bocola M, Wang LW, Sanchis J, Cronin A, Arand M, et al. (2009) Directed evolution of an enantioselective epoxide hydrolase: uncovering the source of enantioselectivity at each evolutionary stage. J Am Chem Soc 131:7334–7343. https://doi.org/10.1021/ja809673d PMID: 19469578

133. Das AK, Bellizzi JJ 3rd, Tandel S, Biehl E, Clardy J, Hofmann SL (2000) Structural basis for the insensitivity of a serine enzyme (palmitoyl-protein thioesterase) to phenylmethylsulfonyl fluoride. J Biol Chem 275:23847–23851. https://doi.org/10.1074/jbc.M002758200 PMID: 10801859

134. Won SJ, Davda D, Labby KJ, Hwang SY, Pricer R, Majmudar JD, et al. (2016) Molecular mechanism for isoform-selective inhibition of acyl protein thioesterases 1 and 2 (APT1 and APT2). ACS Chem Biol 11:3374–3382. https://doi.org/10.1021/acschembio.6b00720 PMID: 27748579

135. Stauch B, Fisher SJ, Cianci M (2015) Open and closed states of *Candida antarctica* lipase B: protonation and the mechanism of interfacial activation. J Lipid Res 56:2348–2358. https://doi.org/10.1194/jlr.M063388 PMID: 26447231

136. Dröge MJ, Boersma YL, van Pouderoyen G, Vrenken TE, Rüggeberg CJ, Reetz MT, et al. (2006) Directed evolution of *Bacillus subtilis* lipase A by use of enantiomeric phosphonate inhibitors: crystal structures and phage display selection. Chembiochem 7:149–157. https://doi.org/10.1002/cbic. 200500308 PMID: 16342303

137. Egloff MP, Marguet F, Buono G, Verger R, Cambillau C, van Tilbeurgh H (1995) The 2.46 Å resolution structure of the pancreatic lipase-colipase complex inhibited by a C11 alkyl phosphonate. Biochemistry 34:2751–2762. https://doi.org/10.1021/bi00009a003 PMID: 7893686

138. Ghosh D, Sawicki M, Lala P, Erman M, Pangborn W, Eyzaguirre J, et al. (2001) Multiple conformations of catalytic serine and histidine in acetylxylan esterase at 0.90 Å. J Biol Chem 276:11159–11166. https://doi.org/10.1074/jbc.M008831200 PMID: 11134051

139. Menyhárd DK, Orgován Z, Szeltner Z, Szamosi I, Harmat V (2015) Catalytically distinct states captured in a crystal lattice: the substrate-bound and scavenger states of acylaminoacyl peptidase and their implications for functionality. Acta Crystallogr D Biol Crystallogr 71:461–472. https://doi.org/10. 1107/S1399004714026819 PMID: 25760596